Ponce, J.; Arago, J.; Vayá Pérez, I.; Gómez Magenti, J.; Tatay, S.; Ortí, E.; Coronado, E. (2016). Photophysical Properties of Oligo(phenylene ethynylene) Iridium(III) Complexes Functionalized with Metal-Anchoring Groups. European Journal of Inorganic Chemistry. (12):1851-1859. https://doi.org/10.1002/ejic.201501409

# Photophysical Properties of Conjugated Iridium(III) Complexes Functionalized with Metal-Anchoring Groups

Julia Ponce,[a] Juan Aragó,[a] Ignacio Vayá,[b] Jorge Gómez Magenti,[b] Sergio Tatay, [a]* Enrique Ortí,[a] and Eugenio Coronado[a]

Dedication ((optional))

**Abstract:** The electrochemical and photophysical properties of a family of conjugated ligands and their iridium(III) cyclometallated complexes are described. They consist of a series of monocationic Ir(III) bis-2-phenylpyridine complexes with *p*-phenylethynyl 1,10-phenanthroline ligands of different length. The structure of these ligands includes terminal groups, acethylthiol or pyridine, which can provide a good electrical contact between metal electrodes. Cyclic voltammetry, absorption and emission spectroscopy, laser flash photolysis, and density functional theory calculations reveal that the high conjugation of the diimine ligand affords small energy gaps between the frontier orbitals. Nevertheless, the nature of the terminal substituents and the extent of the conjugation in the diimine ligand have little influence on the photophysical features at room temperature. The spectroscopic and theoretical calculations agree that the charge transfer nature of the emitting excited state is maintained along the series at room temperature, whereas in rigid matrices ligand-centered states also contribute to the low temperature emission. The good conducting features of the diimine ligands, the small dependence of the HOMO-LUMO gap on the diimine ligands, and the charge transfer nature of the emitting excited state, make these complexes promising test beds for the study of photoconducting phenomena in molecular junctions.

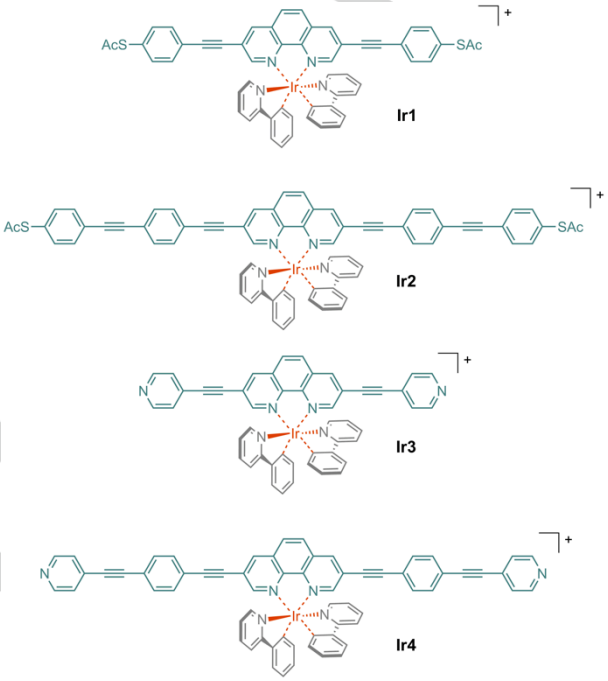


**Figure 1** Chemical structure of the iridium complexes $[Ir(ppy)_2(\mathbf{1–4})]^+$ (**Ir1–Ir4**).

## Introduction

The field of molecular electronics has been recently enriched by the idea of using electromagnetic radiation to modulate molecular junctions response.[1-4] On that basis, the conductance of some single-molecules contacted in between metallic electrodes could be optically switched through light-triggered isomerization.[5-9] On the other hand, molecular dipole changes have demonstrated to have a deep influence on the electronic structure of contacted molecules.[10-12] According to this idea, light has also been proposed as a control tool of molecular conductance in systems that do not undergo photochemical reactions. Along with some experimental work,[13-15] theoretical studies in this area[2, 16-19] support this idea. For example, the effect of illumination on junctions comprising molecules of different lengths[20, 21] or characterized by strong charge-transfer optical transitions[22] have been theoretically studied.

Iridium(III) cyclometallated compounds constitute a focus of intense research due to its unique and tunable photophysical properties. The high spin-orbit coupling of iridium, the largest among all the transition metals,[23] greatly enhances the occurrence of intersystem crossing processes that result in long-lived triplet excited states with intense photoluminescence and high quantum yields.[24] All these features have made Ir(III) complexes highly attractive for a wide sort of applications, such as emitters in organic light-emitting diodes (OLEDs),[25] light-emitting electrochemical cells (LECs),[26] and oxygen sensors.[27] However, to the best of our knowledge, these phosphorescent complexes have never been implemented into single-molecule junctions.

In the prototypical complex $[Ir(ppy)_2(N^\wedge N)]^+$ (Hppy = 2-phenylpyridine and N^N = diimine ligand), the photoluminiscent emission takes place from a triplet metal-to-ligand charge transfer ($^3$MLCT) excited state.[31, 32] Notwithstanding, the nature of the substituents on the diimine ligand has shown to have a marked influence on the luminescent properties of the complexes.[32, 33] For example, triplet ligand-centered ($^3$LC) excited states are found to increase their contribution to the photoluminescence with the conjugation length.[32, 33, 36-40]

In this work, we present the synthesis and characterization of a series of monocationic photoluminiscent Ir(III) complexes (**Ir1**–

[a] Instituto de Ciencia Molecular (ICMol)
Universidad de Valencia
Catedrático José Beltrán 2, 46980 Paterna, Valencia, Spain.
Corresponding Author e-mail: sergio.tatay@uv.es
[b] Departamento de Química
Universitat Politècnica de València
Camino de Vera s/n, 46022 Valencia, Spain

Supporting information for this article is given via a link at the end of the document..

**Ir4**, Figure 1) incorporating conjugated ligands of different molecular length and functionalized with suitable anchoring groups for their integration into metallic molecular junctions.[28, 29] The new compounds result from the combination of iridium(III) bis-cyclometallated 2-phenylpyridine complexes with four different diimine π-conjugated ligands (**1**–**4**). **1**–**4** are 1,10-phenanthroline (phen) derivatives symmetrically functionalized through their 3- and 8- positions with acethylthiol (SAc) and pyridine terminal groups, which are connected to the phen core by phenylethynyl spacers of different length. The molecular conductance of some of these ligands has been already investigated in mechanically controlled break-junctions.[30] Complexes **Ir1**–**Ir4** therefore combine the low resistance features of molecular wires **1**–**4** with the rich photophysics of Ir(III) complexes.

$[Ir(ppy)_2(N^N)]^+$ functionalized with phenylethynyl groups have been reported before.[34, 35] However in the interplay between conjugation and different anchoring groups in **Ir1**–**Ir4** makes difficult to anticipate the nature of the emitting excited state and thus, their behavior on illuminated molecular junctions. This work, for the first time brings together electro- and spectrochemical techniques along with theoretical calculations in the study of iridium(III) bis-cyclometallated 2-phenylpyridine complexes with phenylethynyl substituted diimine ligands. By a

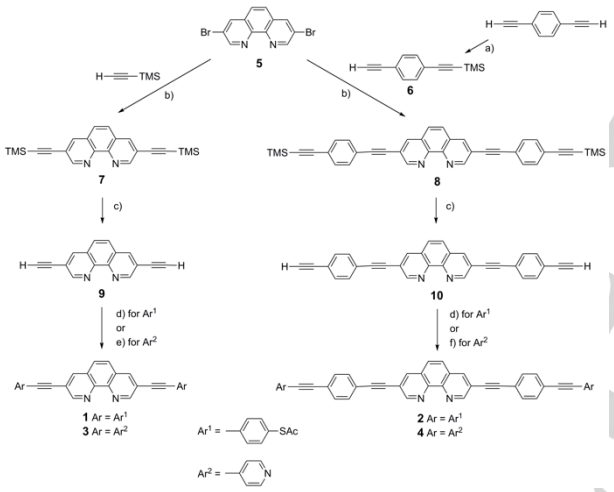

**Scheme 1.** a) *n*-BuLi, TMSCl, THF (68 %); b) $Pd(PPh_3)Cl_2$, CuI, THF, *i*-$Pr_2NH$ (74% for 7, 50% for 8); c) $K_2CO_3$, MeOH (97% for 9, 91% for 10); d) 11 (2 eq.), $Pd(dba)_2$, $PPh_3$, CuI, THF, DIEA (40% for 1, 63% for 2); e) 4-iodopyridine (2 eq.), $Pd(PPh_3)_4$, CuI, THF, DIEA (84% for 3); f) 4-iodopyridine (2 eq.), $Pd(dba)_2$, $PPh_3$, CuI, THF, DIEA (96% for 4). DIEA = N,N-diisopropylethylamine.

thorough combination of all this techniques, we have been able to draw the energy map of the photoexcited states and study the influence of the conjugation length and the nature of the substituents on the photophysical and electrochemical properties of ligands **1**–**4** and complexes **Ir1**–**Ir4**, as a preliminary step towards their integration into light-responsive molecular junctions. Interestingly, compared to previously reported iridium(III) bis-cyclometallated 2-phenylpyridine complexes,[32, 33, 36-40] the HOMO−LUMO gap of the complexes does not follow the expected trend with the extension of the conjugation of the diimine ligand and the nature of the excited state remains unchanged along the series. For that reason, the **Ir1**–**Ir4** family is especially well suited for their study on illuminated molecular junctions.

## Results and Discussion

*Chemical synthesis*

The synthesis of ligands **1**–**4** was accomplished by the sequence of Sonogashira-type cross-coupling reactions, between 3,8-dibromo-1,10-phenanthrolines and substituted phenylacetylenes, displayed in Scheme 1. Ethynyl derivatives **1** and **3** have been previously reported[41, 42] whereas compounds **2** and **4** have been synthesized for the first time. The synthesis of the short molecular wires **1** and **3** was accomplished by coupling 3,8-dibromo-1,10-phenanthroline (**5**)[43] with commercial ethynyltrimethylsilane to afford **7** in good yield. In the case of the

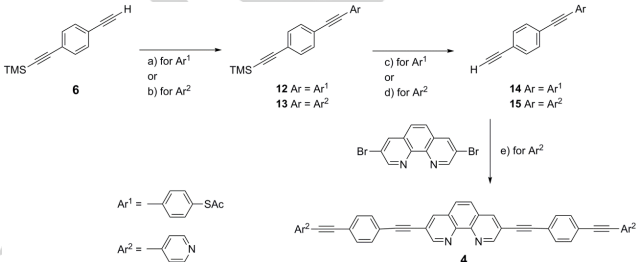

**Scheme 2.** a) **11**, $Pd(PPh_3)_2Cl_2$, CuI, THF, DIEA (43%); b) 4-bromopyridine hydrochloride, $Pd(PPh_3)Cl_2$, CuI, i-$Pr_2NH$ (74%); c) TBAF, AcOH, AcOAc (93%); d) $K_2CO_3$, MeOH, 100%; e) $Pd(PPh_3)_4$, CuI, TEA, THF 60 °C (41%). TEA = triethylamine.

longer ligands **2** and **4**, **5** was coupled with ((4-ethynylphenyl)ethynyl)trimethylsilane (**6**), which had been previously prepared following a reported procedure[44] by the reaction of 1,4-diethynylbenzene with *n*-BuLi in THF and the subsequent addition of chlorotrimethylsilane. Desilylation of **7** and **8** under basic conditions ($K_2CO_3$ in methanol) afforded diethynyl derivatives **9** and **10**, respectively, in high yield.[45] These diethynyl-ended phenanthrolines were then coupled under Sonogashira conditions with two equivalents of 1-(S-acetylthio)-4-iodobenzene (**11**) to afford **1** and **2**, or with commercially available 4-iodopyridine to afford **3** and **4**. Derivative **11** was prepared in high yield by the reduction of 4-iodobenzenesulphonyl chloride.[46]

Alternatively, we tested the route presented in Scheme 2 for the preparation of the longer ligands **2** and **4**. First, compounds **12**[47] and **13**[48] were efficiently prepared by the reaction under standard Sonogashira conditions of **6** with 4-bromopyridine or **11**, respectively.[49, 50] Cleavage of the trimethylsilyl group in pyridine-ended derivative **13** was carried out in basic conditions ($K_2CO_3$ in methanol), whereas compound **12** was deprotected with tetrabutylammonium fluoride (TBAF) in the presence of an excess of acetate in order to avoid the cleavage of the thioacetate group,[50] to yield compounds **14** and **15**, respectively. Molecular rod **4** was synthesized in moderate 24% overall yield from the coupling of dibromophenanthroline **5** with two equivalents of ethynyl derivative **15**. Unfortunately, and although **5** double coupled with **6** (Scheme 1) and **15** (Scheme 2) in moderate yield, the coupling of **5** with two equivalents of **14** did not afford the target molecule **2**.

The preparation of complexes **Ir1**–**Ir4** was carried out starting from the dichloro-bridged Ir(III) dimer $[Ir(ppy)_2Cl]_2$.[51] The treatment of this salt with one equivalent of ligands **1**–**4** in a

refluxing dichloromethane:methanol mixture under inert conditions and the following treatment with an excess of $KPF_6$ afforded monocationic $[Ir(ppy)_2(\mathbf{1–4})][PF_6]$ complexes in reasonable yields (Scheme 3).[32]

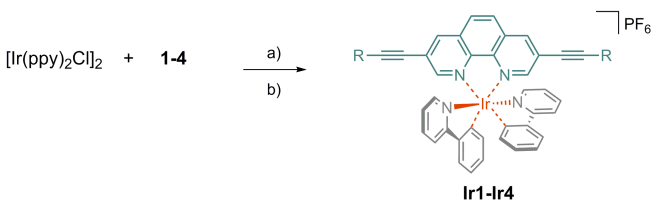


**Scheme 3.** Synthesis of iridium complexes **Ir1–Ir4**: a) $CH_2Cl_2$/MeOH 2:1, reflux; b) $KPF_6$ excess (54% for **Ir1**, 35% for **Ir2**, 40% for **Ir3**, 41% for **Ir4**).

The complexes were characterized by $^1$H nuclear magnetic resonance (NMR), elemental analysis, and high-resolution mass spectrometry (HRMS). In the $^1$H NMR spectra of all complexes (see the Supporting Information), ppy ligands present one set of eight signals each one of them integrating to two protons. This equivalency is consistent with the selective formation of the isomer in which the Ir−$C_{ppy}$ bonds are *trans* to the Ir−$N_{phen}$ bonds according to the so-called '*trans* effect'.[24]

*Electrochemical characterization*

Cyclic voltammograms of **Ir1**–**Ir4** are displayed in Figure 2 and relevant electrochemical data are collected in Table 1. Electrochemical measurements reveal high redox stability with oxidation and reduction half-wave potentials more than 1.8 V apart. All the complexes display oxidation process centered on 1.40 V. This anodic wave has been previously observed in other bis-cyclometallated Ir(III) complexes[32, 33, 36-38, 52] as $[Ir(ppy)_2(phen)]^+$ (1.36 V vs SCE)[32] and has been associated with the bis-cyclometallated Ir(III/IV) oxidation. In agreement with this assignment, the oxidation potential presents minor variations along the **Ir1**–**Ir4** series. The oxidation process looks more irreversible in acetylthiol-ended compounds **Ir1** and **Ir2** than in pyridine-ended derivatives **Ir3** and **Ir4**. The irreversibility of this wave denotes the participation of the ppy moiety in the redox process as supported by previous reports and our theoretical calculations (see below).[53, 54]

At negative potentials, a single cathodic wave is visible between

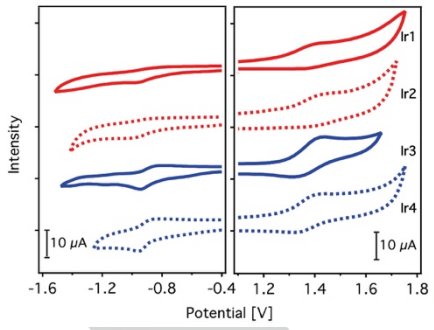


**Figure 2.** Cyclic voltammograms of complexes **Ir1**–**Ir4** in 0.1 M $TBAPF_6$ 1:1 acetonitrile:dichloromethane mixture solutions. Ferrocene was added as internal reference, ($E_{SCE}$ ($Fc^+/Fc^0$) = 0.45 V).[55]

–1.03 and –0.96 V and the ratio between cathodic and anodic peaks is again far from one for **Ir1** and **Ir2**. We attribute this behavior to the high tendency of the ligands to get adsorbed on the electrodes upon reduction,[30] this effect being more pronounced in the case of acetylthiol derivatives than in the pyridine-ended complexes. The potential of the reduction process, particularly in the pyridine-ended derivatives, is found to lay far above from that described for the parent complex $[Ir(ppy)_2(phen)][PF_6]$ ($E_{1/2}$ = –1.28 V vs SCE).[32] This fact suggests that, as mentioned in previous reports[32, 33, 36, 38] and discussed below, the reduction process in **Ir1**–**Ir4** is centered on the N^N ligand.

**Table 1.** Oxidation and reduction potentials vs SCE for **Ir1–Ir4** complexes.

| Compound | $E_c^{red}$ [V] | $E_a^{ox}$ [V] | Electrochemical gap[a] [V] |
|---|---|---|---|
| **Ir1** | –0.96 | +1.39 | 2.35 |
| **Ir2** | –1.03 | +1.39 | 2.42 |
| **Ir3** | –0.94 | +1.42 | 2.36 |
| **Ir4** | –0.95 | +1.40 | 2.35 |
| **fac-Ir(ppy)$_3$** | –2.26[b] | +0.75[c] | |

[a] Electrochemical gaps obtained as the difference between the cathodic peak of the reduction process ($E_c^{red}$) and the anodic peak of the oxidation process ($E_a^{ox}$). [b,c] $E_{1/2}^{red}$ and $E_{1/2}^{ox}$ fac-Ir(ppy)$_3$ data from ref 56 have been added from comparison. Electrochemical measurements were carried out in anhydrous dimethylformamide.

*Photophysical properties*

The absorption spectra in dichloromethane of ligands **1**–**4** along with their iridium complexes **Ir1**–**Ir4** are shown in Figure 4 and the corresponding absorption maxima and molar extinction coefficients are listed in Table 2. Short ligands **1** and **3** exhibited two strong absorption bands, the first peaking at 289 and 283 nm (ε ≈ 55000 $M^{-1}$ $cm^{-1}$) and the second at 351 and 340 nm (ε ≈ 60000 $M^{-1}$ $cm^{-1}$), respectively. These maxima are significantly shifted to lower energies on increasing the conjugation length (ligands **2** and **4**), the bathochromic effect being higher for the pyridine-ended molecular backbones. As in related reported ligands, we assign the lower- and higher-energy bands to long- and short-axis polarized π→π* transitions, respectively.[34, 35, 57]
The absorption bands of the complexes **Ir1**–**Ir4** are broader than those of the bare ligands **1**–**4** (Figure 4 bottom). The spectra show an intense band (ε > 5 × $10^4$ $M^{-1}cm^{-1}$) below 350 nm, a less intense band (ε > 4 × $10^4$ $M^{-1}cm^{-1}$) in the 350–450 nm range. Based on previous reports,[32-34, 36, 38, 40] we assign the first band to π→π* transitions centered on the ppy and phen ligands. The second broad band is the result of the overlap of π→π* LC transitions with spin-allowed $^1$MLCT transitions. In **Ir3**, the latter transitions are distinguishable as a separated band around 400 nm. The red-shift (up to 30 nm) experienced by the bands peaking in the 360–390 nm range compared to those observed for **1**–**4** is in part attributed to the stabilization of the π-electron system of the phen chromophore as a result of the coordination to the cationic Ir(III) center (see below).[57, 58]

**Table 2.** Photophysical properties of ligands **1–4** and complexes **Ir1–Ir4** in dichloromethane and ethanol solutions.

| | $\lambda_{max}$ [nm] $CH_2Cl_2$ ($\varepsilon$) [$10^3$ $M^{-1}cm^{-1}$] | $\lambda_{em}$[a] [nm] $CH_2Cl_2$ 278 K | $\lambda_{em}$[a] [nm] EtOH 278 K | $\lambda_{em}$[a,b] [nm] EtOH 77 K | $E_T$[a,c] [eV] $CH_2Cl_2$ 278 K | $\phi_{air}$ $CH_2Cl_2$ 278 K | $\phi_{Ar}$ $CH_2Cl_2$ 278 K | $\tau$[d] [ns] $CH_2Cl_2$ 278 K | $\tau$[e] [µs] EtOH 77K | $k_r$[f] [$10^6$ $s^{-1}$] $CH_2Cl_2$ 278 K | $k_{nr}$[f] [$10$ $s^{-1}$] $CH_2Cl_2$ 278 K |
|---|---|---|---|---|---|---|---|---|---|---|---|
| **1** | 289 (55),351 (62) | 384 | | 561 | 2.48 | 0.76 | 0.79 | < 1 | | | |
| **2** | 305 (45),367 (74) | 403 | | 568 | 2.37 | 0.83 | 0.84 | < 1 | | | |
| **3** | 283 (57),340 (60) | 384 | | 511 | 2.56 | 0.12 | 0.15 | < 1 | | | |
| **4** | 300 (39),367 (64) | 394 | | 564 | 2.35 | 0.90 | 0.93 | < 1 | | | |
| **Ir1** | 272 (69),380 (46) | 638 | 644 | 562 (552) | 2.22 | 0.097 | 0.151 | 502 | 5.7, 18.8 | 0.30 | 1.7 |
| **Ir2** | 314 (66), 395 (51) | 638 | 644 | 563 (563) | 2.21 | 0.113 | 0.179 | 564 | 4.5, 15.1 | 0.32 | 1.5 |
| **Ir3** | 290 (56), 362 (38) | 648 | 658 | 588 (512) | 2.13 | 0.057 | 0.073 | 202 | 6.7, 18.2 | 0.36 | 4.6 |
| **Ir4** | 301 (53), 389 (51) | 640 | 646 | 566 (566) | 2.19 | 0.049 | 0.073 | 460 | 6.8, 20.6 | 0.16 | 2.0 |
| ***fac*-Ir(ppy)$_3$**[g] | 244 (45), 283 (45) | | 492[g] | 510[g] | | | 0.4 | 1900 | 3.6 | 0.21 | 0.32 |

Concentration is 3 × $10^{-6}$ M. Absorption maxima (λmax), molar attenuation coefficient (ε), emission maxima (λem), triplet energy (ET), fluorescence quantum yield (ϕ), luminesce lifetime ($\tau$), radiative ($k_r$) and non-radiative ($k_{nr}$) emission constants. [a] $\lambda_{exc}$ (**1–4**) = 300 nm, $\lambda_{exc}$ (**Ir1–Ir4**) = 375 nm. [b] Emission maxima registered with a delay of 50 µs for **1–4** and a delay of 5 (50) µs for **Ir1–Ir4**. [c] Determined in deaerated dichloromethane from the 10% rise phosphorescence spectra. [d] Measurements in deaerated dichloromethane solution at the emission maximum ($\lambda_{exc}$ = 375 nm); lifetimes for **1–4** are shorter than 1 ns and could not be resolved by our system. [e] Measurements in deaerated ethanol solid matrix at 560 nm ($\lambda_{exc}$ = 355 nm), lifetimes correspond to a biexponential fit. [f] $k_r$ and $k_{nr}$ in dichloromethane solution were calculated according to the equations: $k_r = \phi_{Ar}/\tau$ and $k_{nr} = (1-\phi_{Ar})/\tau$. [g] *fac*-Ir(ppy)$_3$ data from ref 56 have been added from comparison. In this case emission and lifetime measurements were carried out in 2-methyltetrahydrofuran.

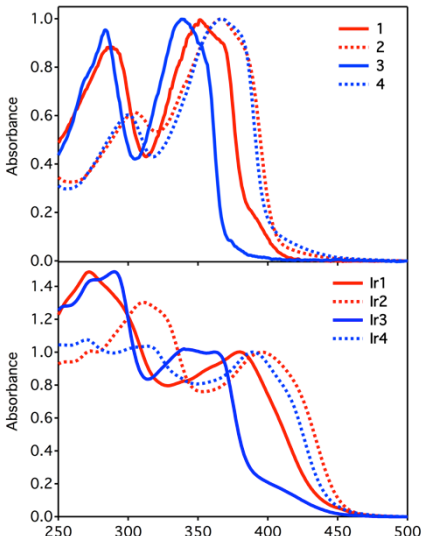


**Figure 4.** Normalized absorption spectra in dichloromethane of ligands **1–4** (top) and complexes **Ir1–Ir4** (bottom). (C = 10–5 M).

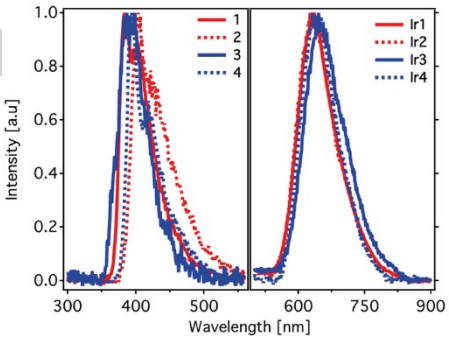


**Figure 3.** Normalized photoluminescence spectra of ligands **1–4** ($l_{exc}$ = 300 nm) and complexes **Ir1–Ir4** ($l_{exc}$ = 375 nm) in dichloromethane at 298 K.

The photoluminescence spectra of ligands **1–4** in dichloromethane at 298 K ($l_{exc}$ = 300 nm) are shown in Figure 3 (left). Emissions are centered in the 380–400 nm range and show relatively high quantum yields (f), which are essentially not affected by the presence of oxygen evidencing the fluorescence character of the emission (Table 2). The emission maxima of ligands **1** and **3** appear at shorter wavelengths than those of **2** and **4**. In addition, the fluorescence quantum yields of the former are lower than those of the more conjugated ligands. Thus, the enhancement of the π-conjugation results in higher ϕ and in a stabilization of the lower energy transitions, in agreement with that observed in the absorption the fluorescence lifetimes ($\tau$) of 1–4 were below 1 ns and could not be resolved by our experimental setup.

The photoluminescence spectra of complexes **Ir1–Ir4** at room temperature are shown in Figure 3 (right) and its photophysical properties are summarized in Table 2. The emission quantum yields of the complexes are much lower than those observed for the bare ligands and are significantly affected by the presence of oxygen. In 10 min air-equilibrated solutions, quantum yields decrease by ~30–40% compared to those of argon-saturated media. In addition, the emission lifetimes of **Ir1–Ir4** at room temperature range in the submicrosecond time scale and are more than two orders of magnitude longer than those found for **1–4** (t < 1 ns). All these features are consistent with the triplet nature of the emissive excited state for all Ir-complexes, according to the

ability of Ir(III) to favor the intersystem crossing from singlet to triplet excited states.

In contrast with that observed for **1**–**4** (Figure 3, left), the shape of the emission of **Ir1**–**Ir4** in dichloromethane solution at 298K is broad and unstructured (Figure 4, right), which is the typical shape expected for emissions from MLCT excited states,[59] and shifts by 6–10 nm towards longer wavelengths in more polar ethanol (Table 2). The emission maxima in dichloromethane are observed around 638–640 nm for **Ir1**, **Ir2**, and **Ir4**, and slightly above for **Ir3** (648 nm). Therefore, and in contrast with that observed in the case of ligands **1**–**4** and with that reported previously,[34, 35, 57, 60] the increase in conjugation length on the diimine ligand does not necessarily lead to an energy decrease of the emission (compare **Ir2** and **Ir4** with **Ir1** and **Ir3**, respectively, in Table 2).

The photoluminescence decay traces of **Ir1**–**Ir4**, measured at the emission maxima in dichloromethane, can be accurately fitted to single exponential functions. The lifetimes resulting from these fittings range from 0.20 to 0.56 ms and are longer for the acetylthiol compounds than for the pyridine-ended derivatives (Table 2). The increase of the conjugation length of the diimine ligand also leads to an increase of the lifetime of **Ir2** and **Ir4** compared with **Ir1** and **Ir3**, respectively. Quantum yields are higher for acetylthiols- than for pyridine-ended derivatives, and all of them are in the range reported for other $[Ir(ppy)_2(N^N)]^+$ complexes with MLCT emissive excited states.[36, 37, 40] The photoluminescence decay traces of **Ir1–Ir4**, measured at the emission maxima in dichloromethane, can be accurately fitted to single exponential functions. The lifetimes resulting from these fittings range from 0.20 to 0.56 ms and are longer for the acetylthiol compounds than for the pyridine-ended derivatives (Table 2). The increase of the conjugation length of the diimine ligand also leads to an increase of the lifetime of **Ir2** and **Ir4** compared with Ir1 and Ir3, respectively. Interestingly, compared to what it is observed at room temperature, the low temperature phosphorescence decay curves measured at 560 nm for **Ir1**–**Ir4** shows a biexponential decay with lifetimes for the two component differing by around 10 μs (Table 2).

The emission spectra of **Ir3** recorded in ethanol glass at different delay times (5 and 50 μs) is shown in Figure 5. In this case, the two components of the emission are well separated in energy and could be clearly resolved. The short-lived (6.7 μs) emission peaking around 600 nm is unstructured and appears blue-shifted by 1800 $cm^{-1}$ compared to room-temperature emission. This behavior is typical of MLCT emitters and originates from the fact that, at low temperature, solvent molecules are frozen in the rigid ethanol matrix and, as a consequence, the emissive $^3$MLCT state is not stabilized by the reorganization of the solvent before emission takes place and the complex emits at higher energies than at room temperature (rigidochromic effect).[59] The long-lived emission (18.2 μs) is structured and peaks at the same energy (512 nm) than that measured for the ligand under equivalent experimental conditions (Table 2). This behavior is characteristic of $^3$LC emissive states, which are

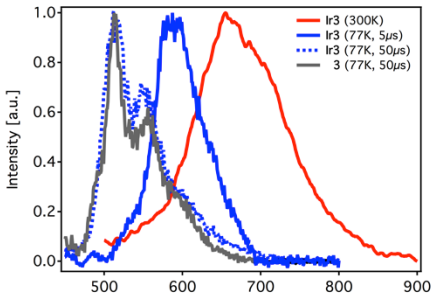


**Figure 5.** Normalized luminescence spectra at $\lambda_{exc}$ = 375 nm of ligand 3 and complex **Ir3** in dichloromethane (300 K) and in ethanol glass (77 K) measured at different delays.

characterized by structured bands whose position is not affected by temperature and usually show longer lifetimes.[24, 33, 38]

Similarly, the emission spectra of **Ir1**, **Ir2**, and **Ir4** shows structured bands whose maxima are close to those found for the low temperature emission of the corresponding ligands (see Figure S1). However, in this case, both components peaks at similar wavelengths (Table 2) and the different contribution to the emission could not be time-resolved. In agreement to that previously observed for other cyclometallated Ir complexes incorporating highly conjugated diimine ligands, although at room temperature the energy of the $^3$LC states is higher that of the $^3$MLCT states, $^3$MLCT states rise in energy at low temperature due to the lack of solvent mobility, and $^3$LC states can increase their contribution to the emission.[60] Thereby, at low temperature **Ir1**–**Ir4** show dual emission from two different triplet states which, according to their lifetime, energy, and shape are assigned to $^3$MLCT and $^3$LC states. Moreover, the good correspondence between the long-lived emission and the emission of the corresponding ligand at low temperature further supports this assignment.

*Transient absorption*

To further investigate the nature and photophysical behavior of the excited states governing the bare ligands and the Ir-complexes at room temperature, laser flash photolysis (LFP) measurements were performed at $\lambda_{exc}$ = 355 nm in deaerated dichloromethane. LFP of **1**–**4** at room temperature affords long-lived absorption species that are highly quenched by oxygen and low-energy triplet acceptors such as b-carotene ($E_T$ = 1.00 eV). On the basis of these observations, the absorption transients are assigned to the triplet $^3$p→p* excited states of the ligands. The transient absorption spectra of **1**–**4** are shown in Figure 6; they are characterized by a broad absorption band throughout the visible region, which extends to the near infrared, with triplet lifetimes ranging from 9.3 to 16.5 ms (see Table 3).

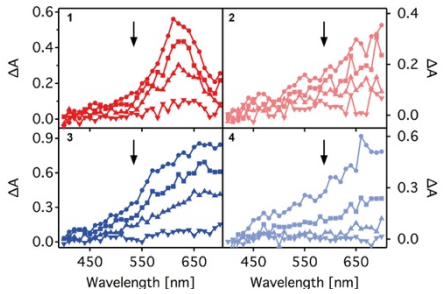


**Figure 6.** Transient absorption spectra of ligands **1**–**4** in deaerated dichloromethane solution at 298 K after excitation at 355 nm. Spectra acquired at 0.4 ms (circle), 4 ms (square), 10 ms (triangle), and 30 ms (inversed triangle) after the laser pulse. The arrows show the evolution of the absorption band in time.

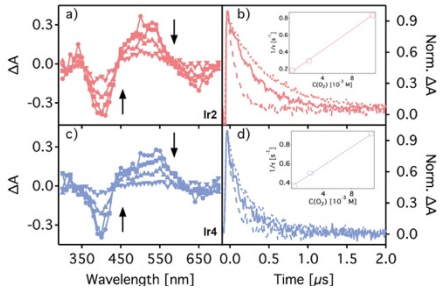


**Figure 7.** Transient absorption spectra in deaerated dichloromethane solution of **Ir2** (a) and **Ir4** (c) recorded at 0.01 ms (circle), 0.1 ms (square), 0.3 ms (triangle), and 1 ms (inverted triangle) after the laser pulse. The arrows show the evolution of the absorption band in time. Decay traces of **Ir2** (b) and **Ir4** (d) monitored at 510 nm in $N_2$ (dot), air (solid), and $O_2$ (dash). The insets show the Stern-Volmer plots of quenching by oxygen. All measurements were performed at 298 K, $l_{exc}$ = 355 nm.

The negative signal at *ca*. 400 nm is assigned to the ground state bleaching, according to the absorption spectra (see Table 2). The absorption species with $l_{max}$ ~ 510 nm are largely quenched by oxygen, with rate constants around 6 × $10^8$ $M^{-1}$ $s^{-1}$ (see Figure 7b and d) and by low-energy triplet acceptors such as b-carotene, thus confirming their triplet nature. Additionally, the decay traces of **Ir1**–**Ir4** at 510 nm can be accurately fitted with a one-order exponential function. The lifetimes range from 0.24 to 0.54 ms and again are found to be higher for acetylthiol-ended compounds than for pyridine-ended derivatives, and are longer-lived for the more conjugated Ir-complexes. It is worth to mention the strong correlation between the lifetime obtained by the laser flash photolysis technique and the photoluminescence decay components detected by emission spectroscopy. This correspondence suggests that the excited state of **Ir1**–**Ir4** from which the photophysical processes (phosphorescence and transient absorption) take place at room temperature corresponds to a $^3$MLCT excited state. In other related Ir(III) complexes, similar transient absorption species ($l_{max}$ ~ 510 nm) were also detected and assigned to $^3$MLCT excited states.[34, 35, 60]

Finally, the bleaching observed around 640 nm is assigned to the photoluminescence detected in the emission spectra measured in deaerated dichloromethane solution at room temperature. (see Table 2)

**Table 3** Photophysical properties of ligands **1–4** and complexes **Ir1–Ir4** derived from the LFP measurements: absorption maxima ($l_{Tmax}$), triplet lifetimes ($t_T$). All measurements were performed in deaerated dichloromethane at room temperature.

| | **1** | **2** | **3** | **4** | **Ir1** | **Ir2** | **Ir3** | **Ir4** |
|---|---|---|---|---|---|---|---|---|
| $l_{Tmax}$**[nm]** | 620 | 700 | 670 | 660 | 510 | 500 | 500 | 540 |
| $t_T$ **[ms]** | 9.3 | 15.8 | 12.4 | 16.5 | 0.43 | 0.54 | 0.24 | 0.27 |

*Theoretical Calculations*

To gain further insight into the electrochemical and photophysical properties of cationic complexes **Ir1**–**Ir4**, density functional theory (DFT) calculations were performed at the B3LYP/(6-31G**+LANL2DZ) level in the presence of dichloromethane (see the computational details). Isolated phenantroline-based ligands **1**–**4** were also computed at the B3LYP/6-31G** level for comparison purposes. Calculations on the electronic ground state ($S_0$) correctly predicts a near-octahedral coordination for the Ir metal and provide geometrical parameters in good agreement with experimental data for similar Ir-based complexes. For instance, the values computed for the Ir−$N_{ppy}$ (2.085 Å), Ir−$C_{ppy}$ (2.023 Å), and Ir−$N_{phen}$ (2.227 Å) bonds in **Ir1** are in good agreement with the experimental X-ray bond lengths (2.04–2.06, 1.99–2.04, and 2.12–2.16 Å, respectively) found for the $[Ir(ppy)_2(3,8\text{-diphenyl-phen})]^+$ complex[39] and with the values reported for $[Ir(piq)_2(phen)]^+$ (piq = 1-phenyl-isoquinoline).[38] The optimized values calculated for the bond distances and the bond angles defining the coordination sphere of the iridium center for all the complexes are collected in Table S1 (see the Supporting Information).

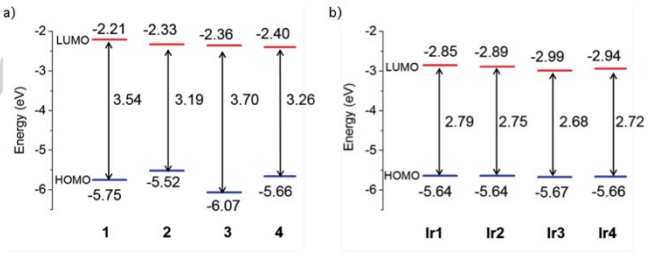


**Figure 7** Energy diagram showing the energies calculated for the HOMOs and LUMOs of (a) ligands **1–4** and (b) complexes **Ir1–Ir4**.

Figure 7 displays the energies calculated for the HOMOs and LUMOs of the phenantroline-based ligands **1**–**4** and complexes **Ir1**–**Ir4**, and Figure 8 shows the isovalue contours computed for the frontier molecular orbitals of **Ir1** and **Ir3** as representative examples. The topology of the molecular orbitals of **Ir2** and **Ir4** (Figure S2) is identical to that of **Ir1**. Similar to other related ppy-based cyclometallated Ir complexes,[38-40] the HOMO is composed of a mixture of Ir(III) dπ orbitals ($t_{2g}$) and phenyl π orbitals with little contributions from the pyridine rings of the cyclometallated ligands. Since the family of complexes **Ir1**–**Ir4** only differs in the diimine ligand, the energy of the HOMO remains almost constant along the series being slightly more stable for **Ir3** and **Ir4** (Figure 7b). Theoretical calculations therefore support the

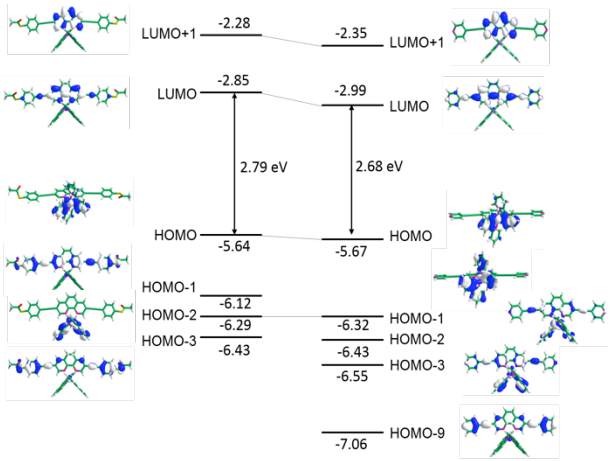


**Figure 8.** Schematic representation showing the isovalue contours (±0.03 a.u.) and the energy values (in eV) calculated for the highest-occupied and lowest-unoccupied molecular orbitals of **Ir1** (left) and **Ir3** (right).

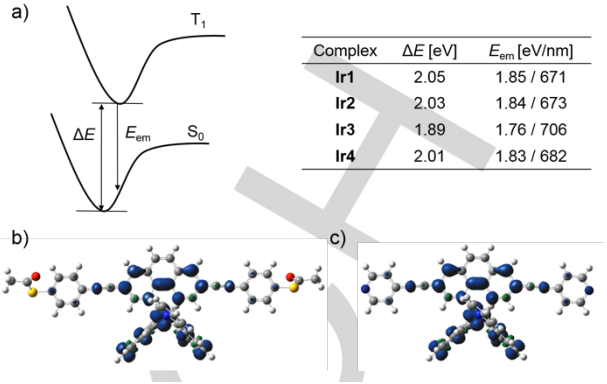


| Complex | $\Delta E$ [eV] | $E_{em}$ [eV/nm] |
|---|---|---|
| **Ir1** | 2.05 | 1.85 / 671 |
| **Ir2** | 2.03 | 1.84 / 673 |
| **Ir3** | 1.89 | 1.76 / 706 |
| **Ir4** | 2.01 | 1.83 / 682 |

**Figure 9.** a) Schematic energy diagram showing the adiabatic energy difference ($\Delta E$) between the $S_0$ and $T_1$ states and the emission energy ($E_{em}$) from $T_1$ calculated for complexes **Ir1–Ir4**. b) and c) Unpaired-electron spin density contours (0.003 a.u.) calculated for the fully relaxed $T_1$ state of **Ir1** and **Ir3**, respectively.

participation of the ppy ligands in the first oxidation process and fully justify the small variation of the oxidation potentials observed on going from **Ir1** (+1.39 V) and **Ir2** (+1.39 V) to **Ir3** (+1.42 V) and **Ir4** (+1.40 V) (Table 1). In contrast to the HOMO, the LUMO is completely localized over the diimine ligands and is mainly centered on the phenanthroline core. Compared with the parent $[Ir(ppy)_2(phen)]^+$ complex with an energy for the LUMO orbital of −2.35 eV,[32] the attachment of phenylethylene groups in 3- and 8- positions of the phen ligand in **Ir1**–**Ir4** leads to an stabilization of the LUMO orbital, and thus, to a reduction of the HOMO−LUMO gap which decreases from 3.18 eV in $[Ir(ppy)_2(phen)]^+$ to about 2.75 eV in **Ir1**–**Ir4**. In agreement with the electrochemical data (Table 1), the energy of the HOMO−LUMO gap is similar for all the complexes.

A wider inspection of the energy position along with the atomic orbital composition at the optimized ground state geometry of the frontier molecular orbitals (Figure 8 and Figure S2) can provide qualitative information about the nature of the low-lying triplet excited states. The lowest-energy triplet electronic transition resulting from the HOMO→LUMO excitation has a MLCT nature mixed with some ligand-to-ligand charge transfer (LLCT) character for all the complexes. Additionally, for complexes **Ir1**, **Ir2**, and **Ir4**, the HOMO-1 is located on the diimine ligands and, thus, a $^3$LC excited state centered on the diimine ligand and described by ~~a~~ the HOMO-1→LUMO one-electron promotion can appear close in energy to the $^3$MLCT state. This effect would be more likely for the more conjugated **Ir2** and **Ir4** complexes (Figure S2), for which both the HOMO-1 and HOMO-2 spread over the diimine ligand and are closer in energy to the HOMO. In contrast to **Ir1**, **Ir2**, and **Ir4**, the HOMO-1 of **Ir3** is localized on the Ir-ppy environment; and the HOMO-2 and HOMO-3, which show some contribution from the diimine skeleton, are significantly stabilized (Figure 8). Thus, $^3$LC excited states for **Ir3** have to be expected to appear at higher energies than in the case of **Ir1**, **Ir2**, and **Ir4**. This analysis of the frontier molecular orbitals supports the well-separated emission from the $^3$LC and $^3$MLCT states observed experimentally for **Ir3** at low temperature (Figure 5).

To characterize in more detail the nature of the emitting excited state, the molecular structure of the lowest triplet excited state ($T_1$) was optimized using the spin-unrestricted UB3LYP approach. After full-geometry relaxation, the $T_1$ state is computed to lay in the range 1.89–2.05 eV above $S_0$ (adiabatic energy differences, $\Delta E$ in Figure 9), in reasonably agreement with the triplet energies experimentally registered from the onset of the phosphorescence (Table 2). As illustrated in Figure 9b and c, the unpaired-electron spin density distribution calculated for **Ir1** and **Ir3** (Ir: 0.48e, ppy: 0.50e, **2**: 1.02e) perfectly matches the topology of the HOMO→LUMO excitation (Figure 8). Similar spin density distributions are found for **Ir2** and **Ir4**. Therefore, calculations clearly indicate that at room temperature the emitting $T_1$ state mainly results from the HOMO→LUMO monoexcitation and implies an electron transfer from the Ir-ppy environment to the conjugated diimine ligand for complexes **Ir1**–**Ir4**. $T_1$ therefore has a $^3$MLCT character with some LLCT contribution in good concordance with the spectroscopic and electrochemical data at room temperature.

To estimate the phosphorescence emission energy, the vertical energy difference between $T_1$ and $S_0$ was computed by performing a single-point calculation of $S_0$ at the optimized minimum-energy geometry of $T_1$ ($E_{em}$ in Table 2a). The calculations predict vertical emission energies in the 1.83–1.85 eV range (682–671 nm) for complexes **Ir1**, **Ir2** and **Ir4**, and a slightly red-shifted emission at 1.76 eV (706 nm) for **Ir3**. The theoretical emission energies follow the same trend that the maxima of the emission bands observed at room temperature, with **Ir1**, **Ir2**, and **Ir4** emitting at almost the same energy and **Ir3** emitting at slightly lower energies (Table 2).

## Conclusions

The synthesis of a family of highly-conjugated, phenanthroline-based diimine ligands, functionalized with suitable terminal groups for their anchoring to metal electrodes, and of its corresponding cyclometallated monocationic Ir(III) complexes has been described. In these complexes, the energy of the LUMO orbital, centered on the diimine ligand, is greatly stabilized by the increased

conjugation of ligands **1**–**4** with respect to bare phen ligand. Accordingly, the electrochemical and photophysical features of **Ir1**–**Ir4** shows lower HOMO−LUMO gaps than the reference complex $[Ir(ppy)_2(phen)][PF_6]$. However, the HOMO−LUMO gap does not follow the expected trend with the extension of the conjugation of the diimine ligand observed in other monocationic Ir(III) complexes, and remains almost unchanged when going from **Ir1** and **Ir3** to the more conjugated **Ir2** and **Ir4**. As a result, the emission wavelength remains almost invariable along the series except for **Ir3**, whose emission is slightly red-shifted with respect to the other complexes. Spectroscopic measurements and DFT calculations agree that the emission of the iridium complexes at room temperature can be unambiguously assigned in all cases to $^3$MLCT excited states. Nevertheless, the contributions of $^3$LC states to the emission have proven to increase in rigid matrices at low temperature. This could be clearly observed in the low-temperature emission of **Ir3**, for which the long-lived component of emission perfectly matches with the emission of ligand **3** at room temperature. According to DFT calculation this behavior arises from the different distribution of **Ir3** HOMO orbitals compared to **Ir1**, **Ir2**, and **Ir4**.

Induced dipolar moments are a pursued feature in molecular electronics. The charge transfer nature of the emitting excited state in complexes **Ir1**–**Ir4**, together with the small dependence of the HOMO−LUMO gap with the molecular length and the substituents (anchoring groups) of the diimine **1**–**4** ligands and the good conducting features reported for ligands **1** and **3** makes the complexes reported herein promising test beds for the study of photoconducting phenomena in molecular junctions. This work represents a first stage into the construction of nanoscale optoelectronic devices with metallic complexes.

## Experimental Section

### Experimental

$^1$H NMR spectra were acquired on a Bruker AVANCE DRX 300 spectrometer. The spectra were referred to residual proton-solvent references. Electrospray mass spectra MS(ES) were obtained with a Waters Micromass ZQ spectrometer in the positive ion mode. Absorption spectra were recorded in dichloromethane solution at $1 \times 10^{-5}$ M concentrations on a Shimadzu UV-2501PC spectrophotometer using 1 cm path length quartz cuvettes. Electrochemical measurements were performed in a nitrogen glove box using an Autolab PGSTAT 128N potentiostat and a three-electrode electrochemical cell consisting in a Glassy carbon working electrode, a platinum wire counter electrode, and a silver wire pseudo-reference electrode.

**Laser Flash Photolysis Measurements.** A pulsed Nd:YAG SL404G-10 Spectron Laser Systems was used at the excitation wavelength of 355 nm. The single pulses were ~10 ns in duration and the energy was lower than 15 mJ/pulse. The detecting light source was a pulsed Lo255 Oriel xenon lamp. The laser flash photolysis system consisted of a pulsed laser, a Xe lamp, a 77200 Oriel monochromator, an Oriel photomultiplier tube (PMT) system made up of a 77348 side-on PMT tube, 70680 PMT housing, and a 70705 PMT power supply. The oscilloscope was a TDS-640A Tektronix. The output signal from the oscilloscope was transferred to a personal computer. All transient measurements were recorded in dichloromethane or ethanol employing $10 \times 10$ mm$^2$ quartz cells with 4 mL capacity and were purged with nitrogen or oxygen for at least 10 min before acquisition. All the experiments were carried out at room temperature.

**Phosphorescence Measurements.** Phosphorescence spectra were obtained from a Photon Technology International (PTI, TimeMaster TM-2/2003) spectrofluorometer equipped with a pulsed Xe lamp. The apparatus was operated in time-resolved mode, with a variable delay time. Compounds were dissolved in ethanol, placed in a quartz tube (5 mm of diameter), and cooled to 77 K. The absorbance of the samples was 0.3 at the excitation wavelength (355 nm).

**Fluorescence Measurements.** Fluorescence decay traces were recorded with an EasyLife X system from OBB with a PTI lifetime detector. The solutions were purged with $N_2$ at least during 10 min. The experiments were performed at room temperature ($l_{exc}$ = 375 nm).

All the chemicals and solvents used were purchased from commercial sources and used without further purification, unless specially mentioned. The starting iridium chloro-bridge dimer $[Ir(ppy)_2Cl]_2$ was prepared according to the literature.[51]

**Computational Details.** Density functional calculations (DFT) were carried out with the D.01 revision of the Gaussian 09 program package[61] using Becke's three-parameter B3LYP exchange-correlation functional[62] together with the 6-31G** basis set for C, H, N, O, and S,[63] and the "double-ζ" quality LANL2DZ basis set for the Ir element.[64] The geometries of the singlet ground state ($S_0$) and of the lowest-energy triplet state ($T_1$) were optimized within the $C_2$ symmetry group. The geometry of the first triplet state was calculated at the spin-unrestricted UB3LYP level with a spin multiplicity of three. All the calculations were performed in the presence of the solvent (dichloromethane). Solvent effects were considered within the self-consistent reaction field (SCRF) theory by using the SMD keyword that performs a polarized continuum model (PCM)[65-67] calculation by using the solvation model of Thrular *et al.*[68] The SMD solvation model is based on the polarized continuous quantum chemical charge density of the solute (the "D" in the name stands for "density").

*3,8-bis((trimethylsilyl)ethynyl)-1,10-phenanthroline,* ***5***

Ethynyltrimethylsilane (0.34 mL, 4 mmol) was added over a degassed mixture of 3,8-dibromo-1,10-phenanthroline (**7**) (0.34 g, 1.0 mmol), CuI (0.02 g, 0.12 mmol), $PdCl_2(PPh_3)_2$ (0.04 g, 0.06 mmol) and diisopropylamine (2 mL) in anhydrous THF (5 mL). The mixture was heated under argon at room temperature for 3 days. Organic solvents were evaporated under reduced pressure and the residue was dissolved in dichloromethane (20 mL) and treated with aqueous KCN (10 mL, 6 g/mL) for 4 hours. The two layers were separated and the aqueous phase was washed with $CH_2Cl_2$ (4 × 15 mL). Combined organic layers were washed with water (4 × 20 mL), dried over $Na_2SO_4$, filtered, and concentrated. The resulting dark solid was chromatographed over silica gel using $CH_2Cl_2$/MeOH as eluent to yield **5** as a brownish solid (0.27 g, 73%).

$^1$H NMR (300 MHz, $CDCl_3$): $\delta$ 9.21 (d, $J$ = 2.0 Hz, 2H), 8.34 (d, $J$ = 2.0 Hz, 2H), 7.76 (s, 2H), 0.32 (s, 18H).

MS (EI): *m*/*z* (%) = 373.5 (100); calcd. for $C_{22}H_{25}N_2Si_2$ [$MH^+$]: 373.2.

*(4-ethynylphenyl)ethynyl)trimethylsilane,* ***6***

A solution of 1,4-diethynylbenzene (2.00 g, 16 mmol) in anhydrous THF (200 mL) was placed in a two neck round-bottom flask under Ar and cooled to –78 °C. n-BuLi was added dropwise (10 mL, 1.6 M in hexane, 16 mmol). After stirring for 1 h at –78 °C, chlorotrimethylsilane (3 mL, 24 mmol) was added dropwise and the solution was then allowed to warm to room temperature overnight. The reaction was quenched with water and THF was eliminated under reduced pressure. Diethyl ether (70 mL) was added, and the organic phase was washed with water and dried over $Na_2SO_4$. Evaporation of the solvent led to a yellow solid composed by 68% of **8**, 12% of the diprotected derivative, and 20% of the starting material. The excess of starting material was evaporated under vacuum and the resulting mixture of mono and diprotected compounds was used in the following stage without further purification.

Compound **6**:

$^1$H NMR ($CDCl_3$, 300 MHz): *δ* 7.41 (s, 4H), 3.15 (s, 1H), 0.25 (s, 9H).

1,4-bis((trimethylsilyl)ethynyl)benzene:

$^1$H NMR ($CDCl_3$, 300 MHz): δ 7.38 (s, 4H), 0.24 (s, 18H).

*3,8-bis((4-((trimethylsilyl)ethynyl)phenyl)ethynyl)-1,10-phenanthroline,* ***8***

The previous mixture of mono and disylilated derivatives (1.62 g, ca. 6.80 mmol of **6**), 3,8-dibromo-1,10-phenanthroline (**5**) (0.92 g, 2.72 mmol), CuI (0.05 g, 0.27 mmol), $PdCl_2(PPh_3)_2$ (0.11 g, 0.16 mmol), DIEA (8 mL), and anhydrous THF (20 mL) were heated under argon at 60 °C for 4 days. The resulting mixture was filtered and the solid washed with $CH_2Cl_2$ (40 mL). The combined organic solutions were washed with water (4 × 15 mL) and dried over $Na_2SO_4$. The solution was filtered and solvent was removed. The resulting solid was chromatographed over silica gel using $CH_2Cl_2$/MeOH as eluent to yield a yellow solid (0.77 g, 50%).

$^1$H NMR (300 MHz, $CDCl_3$): *δ* 9.26 (d, *J* = 2.1 Hz, 2H), 8.36 (d, *J* = 2.1 Hz, 2H), 7.55 and 7.49 (AB system, 8H), 0.26 (s, 18H).

*Molecular rod* ***1***

A mixture of **9** (0.11 g, 0.50 mmol), 1-(acetylthio)-4-iodobenzene (**11**) (0.35 g, 1.25 mmol), CuI (0.05 g, 0.25 mmol), $Pd(dba)_2$ (0.04 g, 0.06 mmol), $PPh_3$ (0.03 g, 0.13 mmol), DIEA (N,N-diisopropylethylamine) (4 mL), and anhydrous THF (10 mL) was stirred under an argon atmosphere at 60 °C for 3 days. The solvents were evaporated and the crude was dissolved in 20 mL of $CH_2Cl_2$ and treated with 10 mL of an aqueous solution of KCN (6 mg/mL) for another 2 hours. Then, the two phases were separated and the aqueous phase was washed four times with $CH_2Cl_2$ (4 × 10 mL). The collected organic phases were washed with water (4 × 15 mL), dried over $Na_2SO_4$, filtered, and concentrated under reduced pressure. The resulting solid was washed with plenty of ether to eliminate the remaining triphenylphosphines and then purified by column chromatography on silica gel using $CH_2Cl_2$/MeOH as eluent to afford **1** as a pale yellow solid (0.105 g, 40%).

$^1$H NMR (300 MHz, $CDCl_3$): *δ* 9.27 (d, *J* = 2.1 Hz, 2H), 8.38 (d, *J* = 2.1 Hz, 2H), 7.80 (s, 2H), 7.65 (d, *J* = 8.6 Hz, 4H), 7.45 (d, *J* = 8.6 Hz, 4H), 2.45 (s, 6H).

MS (EI): *m*/*z* (%) = 529.5 (100); calcd. for $C_{32}H_{20}N_2O_2S_2$ [$MH^+$]: 529.1.

*Molecular rod* ***3***

A mixture of **9** (0.160 g, 0.7 mmol), 4-iodopyridine (0.33 g, 1.61 mmol), CuI (11 mg, 0.06 mmol), $Pd(PPh_3)_4$ (0.08 g, 0.07 mmol), DIEA (3 mL), and anhydrous THF (6 mL) was stirred at 60 °C for 2 days. After evaporation of the solvents, the crude was dissolved in 10 mL of dichloromethane and 5 mL of an aqueous solution of KCN (6 mg/mL) and stirred for another 2 hours. The two phases were separated and the aqueous phase was washed with $CH_2Cl_2$ (4 × 10 mL). The collected organic phases were washed with water (4 × 15 mL), dried over $Na_2SO_4$, filtered, and concentrated affording a yellow solid which was chromatographed over silica gel using $CH_2Cl_2$/MeOH as eluent affording the pure product as a white solid (0.128 g, 84%).

$^1$H NMR (300 MHz, $CDCl_3$): *δ* 9.29 (d, *J* = 2.1 Hz, 2H), 8.67 (d, *J* = 6.0 Hz, 4H), 8.43 (d, *J* = 2.1 Hz, 2H), 7.84 (s, 2H), 7.47 (dd, *J* = 4.4, 1.6 Hz, 4H).

MS (EI): *m*/*z* (%) = 383.3 (100); calcd. for $C_{26}H_{14}N_4$ [$MH^+$]: 383.1.

*3,8-diethynyl-1,10-phenanthroline,* ***9***

A suspension of the bis-silylated phenanthroline **7** (0.27g, 0.73 mmol) and $K_2CO_3$ (0.10 g, 0.73 mmol) in methanol (10 mL) was stirred at room temperature for 1 h. Evaporation of the solvent yielded a solid which was suspended in water, filtered, and washed with plenty of water to afford the pure product as an off-white solid (0.16 g, 97%).

$^1$H NMR (300 MHz, $CDCl_3$): *δ* 9.26 (d, *J* = 2.1 Hz, 2H), 8.39 (d, *J* = 2.1 Hz, 2H), 7.81 (s, 2H), 3.40 (s, 2H).

MS (EI): *m*/*z* (%) = 229.2 (100) calcd. for $C_{16}H_8N_2$ [$MH^+$]: 229.1.

*3,8-bis((4-ethynylphenyl)ethynyl)-1,10-phenanthroline,* ***10***

A suspension of the bis-silylated phenanthroline **8** (0.77 g, 1.35 mmol) and $K_2CO_3$ (0.186 g, 1.35 mmol) in 30 mL of methanol was stirred at room temperature for 1 h. Evaporation of the solvent yielded a solid which was suspended in water, filtered, and washed with plenty of water affording the pure product as an off-white solid (0.50 g, 91%).

$^1$H NMR (300 MHz, $CDCl_3$): *δ* 9.30 (d, *J* = 2.1 Hz, 2H), 8.42 (d, *J* = 2.1 Hz, 2H), 7.84 (s, 2H), 7.60 and 7.55 (AB system, 8H), 3.23 (s, 2H).

*Molecular rod* ***2***

A mixture of **10** (0.21 g, 0.50 mmol), 1-(acetylthio)-4-iodobenzene (**11**) (0.33 g, 1.20 mmol), CuI (0.023 g, 0.12 mmol), $Pd(dba)_2$ (0.034 g, 0.06 mmol), $PPh_3$ (0.063 g, 0.24 mmol), DIEA (4 mL), and anhydrous THF (10 mL) was stirred at 60 °C for 3 days. After evaporation of the solvents, the crude was dissolved in 10 mL of dichloromethane and treated with an aqueous solution of KCN (6 mg/mL, 5 mL) for 2 h. The two phases were separated and the aqueous phase was washed with dichloromethane (4 × 20 mL). The collected organic phases were washed with water (4 × 20 mL), dried over $Na_2SO_4$, filtered, and concentrated affording a yellow

solid that was then suspended in diethyl ether, filtered, and washed with plenty of ether to eliminate the remaining triphenylphosphines. The resulting solid was chromatographed over silica gel using $CH_2Cl_2$/MeOH as eluent to afford the pure product as a yellow solid (0.23 g, 63%).

$^1$H NMR (300 MHz, $CDCl_3$): $\delta$ 9.29 (d, $J$ = 2.0 Hz, 2H), 8.40 (d, $J$ = 2.0 Hz, 2H), 7.82 (s, 2H), 7.64 – 7.52 (m, 12H), 7.42 (d, $J$ = 8.6 Hz, 4H), 2.45 (s, 6H).

HRMS (MALDI): *m*/*z* (%) calcd for $C_{48}H_{28}N_2O_2S_2$: 728.16; found: 727.08 (100) [$M^+$].

*Molecular rod **4***

Method c

A mixture of **10** (0.15 g, 0.35 mmol), 4-iodopyridine (0.18 g, 0.88 mmol), CuI (0.02 g, 0.09 mmol), $Pd(dba)_2$ (0.03 g, 0.04 mmol), $PPh_3$ (0.05 g, 0.18 mmol), DIEA (4 mL), and anhydrous THF (10 mL) was stirred at 60 $^0$C for 7 days. After evaporation of the solvents, the crude was dissolved in 10 mL of dichloromethane and treated with an aqueous solution of KCN (6 mg/mL, 5 mL) for 2 h. The two phases were separated and the aqueous phase was washed with dichloromethane (4 × 20 mL). The collected organic phases were washed with water (4 × 20 mL), dried over Na2SO4, filtered, and concentrated affording a yellow solid that was then suspended in diethyl ether, filtered, and washed with plenty of ether to eliminate the remaining triphenylphosphines. The resulting solid was chromatographed over silica gel using CH2Cl2/MeOH as eluent to afford the pure product as a yellow solid (0.20 g, 96%).

Method e

4-((4-ethynylphenyl)ethynyl)pyridine (**15**) (0.20 g, 0.98 mmol), 3,8-dibromo-1,10-phenanthroline (**5**) (0.11 g, 0.33 mmol), CuI (0.01 g, 0.05 mmol), $Pd(PPh_3)_4$ (0.04 g, 0.03 mmol), and anhydrous THF (15 mL) were heated under argon at 65 ºC for 3 days. The resulting mixture was filtered and the solid washed with dichloromethane (40 mL). The combined organic phases were washed with water (4 × 15 mL), dried over Na2SO4, and concentrated under reduced pressure. The resulting solid was chromatographied over silica gel using CH2Cl2/MeOH as eluent (yellow solid, 0.06 g, 33%).

$^1$H NMR ($CDCl_3$, 300 MHz): $\delta$ 9.30 (d, $J$=2.1 Hz, 2H), 8.64 (d, $J$=6 Hz, 4H), 8.41 (d, $J$=2.1 Hz, 2H), 7.83 (s, 2H), 7.62 (m, 8H), 7.41 (d, $J$=6 Hz, 4H).

MS (ES): *m*/*z* (%) calcd for $C_{42}H_{23}N_4$: 583.66; found: 583.35 (100) [$MH^+$].

*S-(4-((4-((trimethylsilyl)ethynyl)phenyl)ethynyl)phenyl) ethanethioate, **12***

A mixture of 1-(acetylthio)-4-iodobenzene (**11**) (0.33 g, 1.20 mmol), CuI (0.023 g, 0.12 mmol) $PdCl_2(PPh_3)_2$ (0.042 g, 0.06 mmol), DIEA (3 mL), and THF (2 mL) was stirred under argon for 10 min. Addition of the mixture of mono and diprotected ((4-ethynylphenyl)ethynyl)trimethylsilane **6** (0.272g, ca. 1.0 mmol of **6**) turned the color of the mixture into dark. The reaction mixture was refluxed for 3 days. Dichloromethane (50 mL) was added, and the organic phase was washed with water (4 × 20 mL) and dried over $Na_2SO_4$. Organic solvents were removed under reduced pressure and the resulting brown solid was purified by silica column chromatography (hexane/CH2Cl2), affording the pure product as a yellow solid (0.15 g, 43%).

$^1$H NMR (300 MHz, $CDCl_3$): $\delta$ 7.54 (d, $J$ = 8.6 Hz, 2H), 7.45 (s, 4H), 7.40 (d, $J$ = 8.6 Hz, 2H), 2.44 (s, 3H), 0.26 (s, 9H).

*4-((4-((trimethylsilyl)ethynyl)phenyl)ethynyl)pyridine, **13***

4-Bromopyridine hydrochloride (0.36 g, 1.86 mmol) was placed in a conical bottom flask under Ar and stirred under argon for 10 min with i-$Pr_2$NH (6 mL), CuI (0.01 g, 0.04 mmol), and $PdCl_2(PPh_3)_2$ (0.03 g, 0.04 mmol). The color of the mixture changed from green to yellow. Addition of the mixture of ((4-ethynylphenyl)ethynyl)trimethylsilane **6** and the diprotected 1,4-bis((trimethylsilyl)ethynyl)benzene (0.33 g, ca.1.69 mmol of **6**) turned the color into dark. After 24 hours of stirring at 40 °C, 50 mL of CH2Cl2 were added to the reaction mixture. The organic phase was washed with water (4 × 20 mL), dried over $Na_2SO_4$, and concentrated under reduced pressure. The resulting brown solid was purified by silica column chromatography (hexane/ diethyl ether, 8:2), giving a yellow crystalline solid (0.34 g, 74%).

$^1$H NMR ($CDCl_3$, 300 MHz): $\delta$ 8.62 (d, $J$=6 Hz, 2H), 7.45 (s, 4H), 7.42 (d, $J$=6 Hz, 2H), 0.26 (s, 9H).

*S-(4-((4-ethynylphenyl)ethynyl)phenyl) ethanethioate, **14***

Compound **12** (0.65 g, 1.87 mmol), THF (10 mL), acetic anhydride (0.35 mL, 3.74 mmol), acetic acid (0.22 mL, 3.74 mmol), and tetrabutylammonium fluoride (2.1 mL of a 1.0 M solution in THF) were stirred together under argon overnight. Dichloromethane (40 mL) was added and the organic phase was washed with water (4 × 20 mL) and dried over $Na_2SO_4$. Organic solvents were removed under reduced pressure to afford the pure product as a yellow solid (0.50 g, 93%).

$^1$H NMR (300 MHz, CDCl3): $\delta$ 7.56 (d, $J$ = 8.1 Hz, 2H), 7.49 (s, 4H), 7.41 (d, $J$ = 8.1 Hz, 2H), 3.19 (s, 1H), 2.44 (s, 3H).

*4-((4-ethynylphenyl)ethynyl)pyridine, **15***

A solution of **13** (0.15 g, 0.54 mmol) in 25 mL of methanol was stirred for 1 h with 0.10 g (0.76 mmol) of $K_2CO_3$. Solvent was removed and the resulting solid was uptaken in diethyl ether (60 mL) and washed with brine (2 × 20 mL) and water (2 × 20 mL). The organic solvent was evaporated affording the pure product in quantitative yield (0.11 g, 0.54 mmol).

1H NMR (CDCl3, 300 MHz): $\delta$ 8.62 (d, $J$=6 Hz, 2H), 7.50 (s, 4H), 7.42 (d, $J$=6 Hz, 2H), 3.21 (s, 1H).

MS (ES): *m*/*z* (%): calcd. for C15H10N: 204.08; found: 204.23 (100) [$MH]^+$.

*General procedure for the preparation of the iridium complexes*

A mixture of $[Ir(ppy)_2Cl]_2$ (0.05 mmol) and **1**–**4** (0.1 mmol) was dissolved in a dichloromethane: methanol mixture (12 mL, 2:1 v/v) and heated under reflux for 24 h. Evaporation of the solvents afforded a red solid which was redissolved in dichloromethane. An excess of $KPF_6$ (1 mmol) was added, and the residue was filtered in order to eliminate the remaining inorganic salts. The resulting solution was evaporated under reduced pressure and the solid was purified by silica column chromatography ($CH_2Cl_2$/ MeOH 1%) affording the pure products as a bright orange solids.

***Ir1*** (54%)

$^1$H NMR (300 MHz, $CD_2Cl_2$): $\delta$ 8.72 (d, $J$ = 1.8 Hz, 2H), 8.37 (d, $J$ = 1.8 Hz, 2H), 8.21 (s, 2H), 8.00 (d, $J$ = 8.0 Hz, 2H), 7.85 – 7.72 (m, 4H), 7.58 (d, $J$ = 8.5 Hz, 4H), 7.47 (d, $J$ = 8.5 Hz, 4H), 7.40 (d, $J$ = 7.5 Hz, 2H),7.15 (td, $J$ = 7.5, 1.2 Hz, 2H), 7.02 (td, $J$ = 7.5, 1.2 Hz, 2H), 6.91 (td, $J$ = 7.5, 1.2 Hz, 2H), 6.40 (dd, $J$ = 7.5, 1.2 Hz, 2H), 2.44 (s, 6H).

MS (ES): *m*/*z* (%): calcd. for $C_{54}H_{36}N_4IrO_2S_2$: 1029.19; found: 1029.45 (100) $[Ir(ppy)(\mathbf{1})]^+$. HRMS (MALDI): *m*/*z* (%): calcd. for $C_{54}H_{36}N_4IrO_2S_2$: 1029.19; found: 1028.98 (100) $[Ir(ppy)(\mathbf{1})]^+$.

Elemental analysis (%) calcd. For $IrC_{54}F_6H_{36}N_4O_2PS_2$: C, 55.24; H, 3.09; N, 4.77; S, 5.46; Found: C, 55.16; H, 3.10; N, 4.74; S, 5.49.

***Ir2*** (35%)

$^1$H NMR (300 MHz, $CD_2Cl_2$): $\delta$ 8.71 (d, $J$ = 1.8 Hz, 2H), 8.39 (d, $J$ = 1.8 Hz, 2H), 8.20 (s, 2H), 8.01 (d, $J$ = 8.0 Hz, 2H), 7.85-7.72 (m, 4H), 7.60-7.53 (m, 12H), 7.47 – 7.38 (m, 6H), 7.17 (td $J$ = 7.5, 1.2 Hz, 2H), 7.04 (td $J$ = 7.5, 1.2 Hz, 2H), 6.91 (td $J$ = 7.5, 1.2 Hz, 2H), 6.41 (d, $J$ = 7.5 Hz, 2H), 2.44 (s, 6H).

HRMS (MALDI): *m*/*z* (%): calcd. for $C_{70}H_{44}N_4IrO_2S_2$: 1229.25; found: 1228.95 (100) $[Ir(ppy)(\mathbf{2})]^+$.

Elemental analysis (%) calcd. For $IrC_{70}F_6H_{44}N_4O_2PS_2$: C, 61.17; H, 3.23; N, 4.08; S, 4.67; Found: C, 61.10; H, 3.20; N, 4.04; S, 4.60.

MS (ES): *m*/*z* (%): calcd. for $C_{70}H_{44}N_4IrO_2S_2$: 1229.25; found: 1229.30 (100) $[Ir(ppy)(\mathbf{2})]^+$.

***Ir3*** (40%)

$^1$H NMR (300 MHz, $CD_2Cl_2$): $\delta$ 8.79 (d, $J$ = 1.8 Hz, 2H), 8.64 (d, $J$ = 6.0 Hz, 4H), 8.39 (d, $J$ = 1.8 Hz, 2H), 8.26 (s, 2H), 8.00 (d, $J$ = 8.0 Hz, 2H), 7.85 – 7.72 (m, 4H), 7.40 (m, 6H), 7.15 (td, $J$ = 7.5, 1.2 Hz, 2H), 7.02 (td, $J$ = 7.5, 1.2 Hz, 2H), 6.92 (td, $J$ = 7.5, 1.2 Hz, 2H), 6.39 (dd, $J$ = 7.5, 1.2 Hz, 2H).

HRMS (MALDI): *m*/*z* (%): calcd. for $C_{48}H_{30}N_6Ir$: 883.22; found: 883.17 (100) $[Ir(ppy)(\mathbf{3})]^+$.

Elemental analysis (%) calcd. For $IrC_{48}F_6H_{30}N_6P$: C, 56.08; H, 2.94; N, 8.18; Found: C, 56. 05; H, 2.93; N, 8.12.

***Ir4*** (41%)

$^1$H NMR (300 MHz, $CD_2Cl_2$): $\delta$ 8.73 (d, $J$ = 1.8 Hz, 2H), 8.61 (d, $J$ = 6.0 Hz, 4H), 8.38 (d, $J$ = 1.8 Hz, 2H), 8.22 (s, 2H), 8.01 (d, $J$ = 8.0 Hz, 2H), 7.82- 7.78 (m, 4H), 7.58 (m, 8H), 7.41-7.39 (m, 6H), 7.16 (td, J = 7.5, 1.2 Hz, 2H), 7.03 (td, J = 7.5, 1.2 Hz, 2H), 6.91 (td, J = 7.5, 1.2 Hz, 2H), 6.41 (dd, J = 7.5, 1.2 Hz, 2H).

HRMS (MALDI): *m*/*z* (%): calcd. for $C_{64}H_{38}N_6Ir$: 1083.28; found: 1038.31 (100) $[Ir(ppy)(\mathbf{4})]^+$.

Elemental analysis (%) calcd. for $IrC_{64}F_6H_{38}N_6P$: C, 62.59; H, 3.12; N, 6.84; Found: C, 62.56; H, 3.10; N, 6.82.

## Acknowledgements

Authors would like to specially acknowledge Prof. Hans U. Güdel for his valuable input and invaluable friendship. The present work has been funded by the EU (ERC Advanced Grant SPINMOL), the Spanish MINECO co-financied by FEDER (Projects CTQ2012-31914, MAT2014-56143 and CONSOLIDER-INGENIO in Molecular Nanoscience), the "Generalitat Valenciana" (Prometeo/2012/053, PrometeoII/2013/006 and ISIC-Nano). J.P, I.V and S.T thank the MICINN for their predoctoral fellowship and JdlC contracts. J.A, I.V and S.T also thank the EU for their FP7-PEOPLE-2012-IEF-329513, PCIG12GA-2012-334257 and MSCA-IF-657465, and FP7-PEOPLE-2012-CIG-321739 grants repectively..

**Keywords** Iridium • photophysical properties • density functional calculations • anchoring groups • molecular junctions

(1) Shamai, T.; Selzer, Y. *Chem. Soc. Rev.* **2011**, *40*, 2293-2305.

(2) Galperin, M.; Nitzan, A. *Phys. Chem. Chem. Phys.* **2012**, *14*, 9421-9438.

(3) Aradhya, S. V.; Venkataraman, L. *Nat. Nanotechnol.* **2013**, *8*, 399-410.

(4) Rigaut, S. *Dalton Trans.* **2013**, *42*, 15859-15863.

(5) Dulić, D.; Van Der Molen, S. J.; Kudernac, T.; Jonkman, H. T.; De Jong, J. J. D.; Bowden, T. N.; Van Esch, J.; Feringa, B. L.; Van Wees, B. J. *Phys. Rev. Lett.* **2003**, *91*, 207402/1-207402/4.

(6) Whalley, A. C.; Steigerwald, M. L.; Guo, X.; Nuckolls, C. *J. Am. Chem. Soc.* **2007**, *129*, 12590-12591.

(7) Tam, E. S.; Parks, J. J.; Shum, W. W.; Zhong, Y. W.; Santiago-Berríos, M. B.; Zheng, X.; Yang, W.; Chan, G. K. L.; Abruña, H. D.; Ralph, D. C. *ACS Nano* **2011**, *5*, 5115-5123.

(8) Lara-Avila, S.; Danilov, A. V.; Kubatkin, S. E.; Broman, S. L.; Parker, C. R.; Nielsen, M. B. *J. Phys. Chem. C* **2011**, *115*, 18372-18377.

(9) Kim, Y.; Hellmuth, T. J.; Sysoiev, D.; Pauly, F.; Pietsch, T.; Wolf, J.; Erbe, A.; Huhn, T.; Groth, U.; Steiner, U. E.; Scheer, E. *Nano Lett.* **2012**, *12*, 3736-3742.

(10) Elbing, M.; Ochs, R.; Koentopp, M.; Fischer, M.; Von Hänisch, C.; Weigend, F.; Evers, F.; Weber, H. B.; Mayor, M. *Proc. Natl. Acad. Sci. U. S. A.* **2005**, *102*, 8815-8820.

(11) Lee, Y.; Yuan, S.; Yu, L. *Sci. China: Chem.* **2011**, *54*, 410-414.

(12) Jiang, P.; Morales, G. M.; You, W.; Yu, L. *Angew. Chem., Int. Ed.* **2004**, *43*, 4471-4475.

(13) Battacharyya, S.; Kibel, A.; Kodis, G.; Liddell, P. A.; Gervaldo, M.; Gust, D.; Lindsay, S. *Nano Lett.* **2011**, *11*, 2709-2714.

(14) Gerster, D.; Reichert, J.; Bi, H.; Barth, J. V.; Kaniber, S. M.; Holleitner, A. W.; Visoly-Fisher, I.; Sergani, S.; Carmeli, I. *Nat. Nanotechnol.* **2012**, *7*, 673-676.

(15) Vadai, M.; Nachman, N.; Ben-Zion, M.; Bürkle, M.; Pauly, F.; Cuevas, J. C.; Selzer, Y. *J. Phys. Chem. Lett.* **2013**, *4*, 2811-2816.

(16) Parker, S. M.; Smeu, M.; Franco, I.; Ratner, M. A.; Seideman, T. *Nano Lett.* **2014**, *14*, 4587-4591.

(17) Löfas, H.; Jahn, B. O.; Wärna, J.; Emanuelsson, R.; Ahuja, R.; Grigoriev, A.; Ottosson, H. *Faraday Discuss.* **2014**, *174*, 105-124.

(18) Hsu, L. Y.; Xie, D.; Rabitz, H. *J. Chem. Phys.* **2014**, *141*, 124703.

(19) Cao, H.; Zhang, M.; Tao, T.; Song, M.; Zhang, C. *J. Chem. Phys.* **2015**, *142*, 084705.

(20) Viljas, J. K.; Pauly, F.; Cuevas, J. C. *Phys. Rev. B: Condens. Matter Mater. Phys.* **2007**, *76*, 033403.

(21) Viljas, J. K.; Pauly, F.; Cuevas, J. C. *Phys. Rev. B: Condens. Matter Mater. Phys.* **2008**, *77*, 155119.

(22) Galperin, M.; Nitzan, A. *J. Chem. Phys.* **2006**, *124*, 234709.

(23) Cotton, F. A.; Wilkinson, G. In *Advanced inorganic chemistry: a comprehensive text;* Wyley: New York, 1980; .

(24) Flamigni, L.; Barbieri, A.; Sabatini, C.; Ventura, B.; Barigelletti, F. *Top. Curr. Chem.* **2007**, *281*, 143-203.

(25) Evans, R. C.; Douglas, P.; Winscom, C. J. *Coord. Chem. Rev.* **2006**, *250*, 2093-2126.

(26) Costa, R. D.; Ortí, E.; Bolink, H. J.; Monti, F.; Accorsi, G.; Armaroli, N. *Angew. Chem. , Int. Ed.* **2012**, *51*, 8178-8211.

(27) Ruggi, A.; van Leeuwen, F. W. B.; Velders, A. H. *Coord. Chem. Rev.* **2011**, *255*, 2542-2554.

(28) Huber, R.; González, M. T.; Wu, S.; Langer, M.; Grunder, S.; Horhoiu, V.; Mayor, M.; Bryce, M. R.; Wang, C.; Jitchati, R.; Schönenberger, C.; Calame, M. *J. Am. Chem. Soc.* **2008**, *130*, 1080-1084.

(29) Hong, W.; Manrique, D. Z.; Moreno-García, P.; Gulcur, M.; Mishchenko, A.; Lambert, C. J.; Bryce, M. R.; Wandlowski, T. *J. Am. Chem. Soc.* **2012**, *134*, 2292-2304.

(30) Ponce, J.; Arroyo, C. R.; Tatay, S.; Frisenda, R.; Gaviña, P.; Aravena, D.; Ruiz, E.; Van Der Zant, H. S. J.; Coronado, E. *J. Am. Chem. Soc.* **2014**, *136*, 8314-8322.

(31) Ohsawa, Y.; Sprouse, S.; King, K. A.; DeArmond, M. K.; Hanck, K. W.; Watts, R. J. *J. Phys. Chem.* **1987**, *91*, 1047-1054.

(32) Dragonetti, C.; Falciola, L.; Mussini, P.; Righetto, S.; Roberto, D.; Ugo, R.; Valore, A.; De Angelis, F.; Fantacci, S.; Sgamellotti, A.; Ramon, M.; Muccini, M. *Inorg. Chem.* **2007**, *46*, 8533-8547.

(33) Lo, K. K. W.; Chung, C. K.; Lee, T. K. M.; Lui, L. H.; Tsang, K. H. K.; Zhu, N. *Inorg. Chem.* **2003**, *42*, 6886-6897.

(34) Glusac, K. D.; Jiang, S.; Schanze, K. S. *Chem. Commun.* **2002**, *8*, 2504-2505.

(35) Kim, K. Y.; Farley, R. T.; Schanze, K. S. *J. Phys. Chem. B* **2006**, *110*, 17302-17304.

(36) Neve, F.; La Deda, M.; Crispini, A.; Bellusci, A.; Puntoriero, F.; Campagna, S. *Organometallics* **2004**, *23*, 5856-5863.

(37) Lepeltier, M.; Lee, T. K. M.; Lo, K. K. W.; Toupet, L.; Le Bozec, H.; Guerchais, V. *Eur. J. Inorg. Chem.* **2005**, 110-117.

(38) Zhao, Q.; Liu, S.; Shi, M.; Wang, C.; Yu, M.; Li, L.; Li, F.; Yi, T.; Huang, C. *Inorg. Chem.* **2006**, *45*, 6152-6160.

(39) Zeng, X.; Tavasli, M.; Perepichka, I. F.; Batsanov, A. S.; Bryce, M. R.; Chiang, C. J.; Rothe, C.; Monkman, A. P. *Chem. -Eur. J.* **2008**, *14*, 933-943.

(40) Kiran, R. V.; Hogan, C. F.; James, B. D.; Wilson, D. J. D. *Eur. J. Inorg. Chem.* **2011**, 4816-4825.

(41) Resendiz, M. J. E.; Noveron, J. C.; Disteldorf, H.; Fischer, S.; Stang, P. J. *Org. Lett.* **2004**, *6*, 651-653.

(42) Ciszek, J. W.; Tour, J. M. *Tetrahedron Lett.* **2004**, *45*, 2801-2803.

(43) Saitoh, Y.; Koizumi, T.; Osakada, K.; Yamamoto, T. *Can. J. Chem.* **1997**, *75*, 1336-1339.

(44) Huang, S.; Tour, J. M. *J. Org. Chem.* **1999**, *64*, 8898-8906.

(45) Ziessel, R.; Suffert, J.; Youinou, M. *J. Org. Chem.* **1996**, *61*, 6535-6546.

(46) Gryko, D. T.; Clausen, C.; Roth, K. M.; Dontha, N.; Bocian, D. F.; Kuhr, W. G.; Lindsey, J. S. *J. Org. Chem.* **2000**, *65*, 7345-7355.

(47) Nielsen, M.; Gothelf, K. V. *J. Chem. Soc. , Perkin Trans. 1* **2001**, *19*, 2440-2444.

(48) Wu, I.; Lin, J. T.; Luo, J.; Sun, S.; Li, C.; Lin, K. J.; Tsai, C.; Hsu, C.; Lin, J. *Organometallics* **1997**, *16*, 2038-2048.

(49) Holmes, B. T.; Pennington, W. T.; Hanks, T. W. *Synth. Commun.* **2003**, *33*, 2447-2461.

(50) Flatt, A. K.; Yao, Y.; Maya, F.; Tour, J. M. *J. Org. Chem.* **2004**, *69*, 1752-1755.

(51) Sprouse, S.; King, K. A.; Spellane, P. J.; Watts, R. J. *J. Am. Chem. Soc.* **1984**, *106*, 6647-6653.

(52) Zhao, L.; Ghosh, K.; Zheng, Y.; Lyndon, M. M.; Williams, T. I.; Stang, P. J. *Inorg. Chem.* **2009**, *48*, 5590.

(53) Neve, F.; Crisping, A.; Campagna, S.; Serroni, S. *Inorg. Chem.* **1999**, *38*, 2250-2258.

(54) Didier, P.; Ortmans, I.; Mesmaeker, A. K. -.; Watts, R. J. *Inorg. Chem.* **1993**, *32*, 5239-5245.

(55) Bao, D.; Millare, B.; Xia, W.; Steyer, B. G.; Gerasimenko, A. A.; Ferreira, A.; Contreras, A.; Vullev, V. I. *J. Phys. Chem. A* **2009**, *113*, 1259-1267.

(56) Tamayo, A. B.; Alleyne, B. D.; Djurovich, P. I.; Lamansky, S.; Tsyba, I.; Ho, N. N.; Bau, R.; Thompson, M. E. *J. Am. Chem. Soc.* **2003**, *125*, 7377-7387.

(57) Walters, K. A.; Ley, K. D.; Cavalaheiro, C. S. P.; Miller, S. E.; Gosztola, D.; Wasielewski, M. R.; Bussandri, A. P.; Van Willigen, H.; Schanze, K. S. *J. Am. Chem. Soc.* **2001**, *123*, 8329-8342.

(58) Manas, E. S.; Chen, L. X. *Chem. Phys. Lett.* **2000**, *331*, 299-307.

(59) Juris, A.; Balzani, V.; Barigelletti, F.; Campagna, S.; Belser, P.; von Zelewsky, A. *Coord. Chem. Rev.* **1988**, *84*, 85-277.

(60) Lafolet, F.; Welter, S.; Popovic, Z.; De Cola, L. *J. Mater. Chem.* **2005**, *15*, 2820-2828.

(61) Frisch, M. J.; Trucks, G. W.; Schlegel, H. B.; Scuseria, G. E.; Robb, M. A.; Cheeseman, J. R.; Scalmani, G.; Barone, V.; Mennucci, B.; Petersson, G. A.; Nakatsuji, H.; Caricato, M.; Li, X.; Hratchian, H. P.; Izmaylov, A. F.; Bloino, J.; Zheng, G.; Sonnenberg, J. L.; Hada, M.; Ehara, M.; Toyota, K.; Fukuda, R.; Hasegawa, J.; Ishida, M.; Nakajima, T.; Honda, Y.; Kitao, O.; Nakai, H.; Vreven, T.; Montgomery, J. A., Jr.; Peralta, J. E.; Ogliaro, F.; Bearpark, M.; Heyd, J. J.; Brothers, E.; Kudin, K. N.; Staroverov, V. N.; Kobayashi, R.; Normand, J.; Raghavachari, K.; Rendell, A.; Burant, J. C.; Iyengar, S. S.; Tomasi, J.; Cossi, M.; Rega, N.; Millam, N. J.; Klene, M.; Knox, J. E.; Cross, J. B.; Bakken, V.; Adamo, C.; Jaramillo, J.; Gomperts, R.; Stratmann, R. E.; Yazyev, O.; Austin, A. J.; Cammi, R.; Pomelli, C.; Ochterski, J. W.; Martin, R. L.; Morokuma, K.; Zakrzewski, V. G.; Voth, G. A.; Salvador, P.; Dannenberg, J. J.; Dapprich, S.; Daniels, A. D.; Farkas, Ö.; Foresman, J. B.; Ortiz, J. V.; Cioslowski, J.; Fox, D. J. In *Gaussian 09, Revision D.01;* Gaussian, Inc.: Wallingford CT, 2009; .

(62) Lee, C.; Yang, W.; Parr, R. G. *Phys. Rev. B* **1988**, *37*, 785-789.

(63) Francl, M. M.; Pietro, W. J.; Hehre, W. J.; Binkley, J. S.; Gordon, M. S.; DeFrees, D. J.; Pople, J. A. *J. Chem. Phys.* **1982**, *77*, 3654-3665.

(64) Hay, P. J.; Wadt, W. R. *J. Chem. Phys.* **1985**, *82*, 299-310.

(65) Tomasi, J.; Persico, M. *Chem. Rev.* **1994**, *94*, 2027-2094.

(66) Tomasi, J.; Mennucci, B.; Cammi, R. *Chem. Rev.* **2005**, *105*, 2999-3093.

(67) Cramer, C. S.; Truhlar, D. G. In *Solvent Effects and Chemical Reactivity;* Kluwer, Dordrecht, 1996; , pp 1–80.

(68) Marenich, A. V.; Cramer, C. J.; Truhlar, D. G. *J. Phys. Chem. B* **2009**, *113*, 6378-6396.

**Entry for the Table of Contents** (Please choose one layout)

# FULL PAPER

Text for Table of Contents

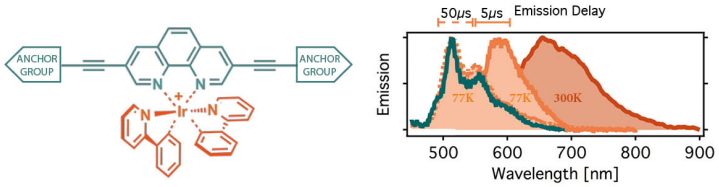


**Iridium Photophysics**

*Julia Ponce, Juan Aragó, Ignacio Vayá, Jorge Gomez Magenti, Sergio Tatay,* Enrique Ortí, and Eugenio Coronado*

***Page No. – Page No.***

**Photophysical Properties of Conjugated Iridium(III) Complexes Functionalized with Metal-Anchoring Groups**

# Supporting Information

## Photophysical properties of conjugated Iridium (III) complexes functionalized with metal anchoring groups

*Julia Ponce,† Juan Aragó,† Ignacio Vayá,# Jorge Gómez,† Sergio Tatay,† Enrique Ortí,† and Eugenio Coronado†*

† Instituto de Ciencia Molecular (ICMol), Universidad de Valencia, Catedrático José Beltrán 2, 46980 Paterna, Valencia, Spain. E-mail: sergio.tatay@uv.es

# Departamento de Química, Universitat Politècnica de València, Camino de Vera s/n. 46022 Valencia

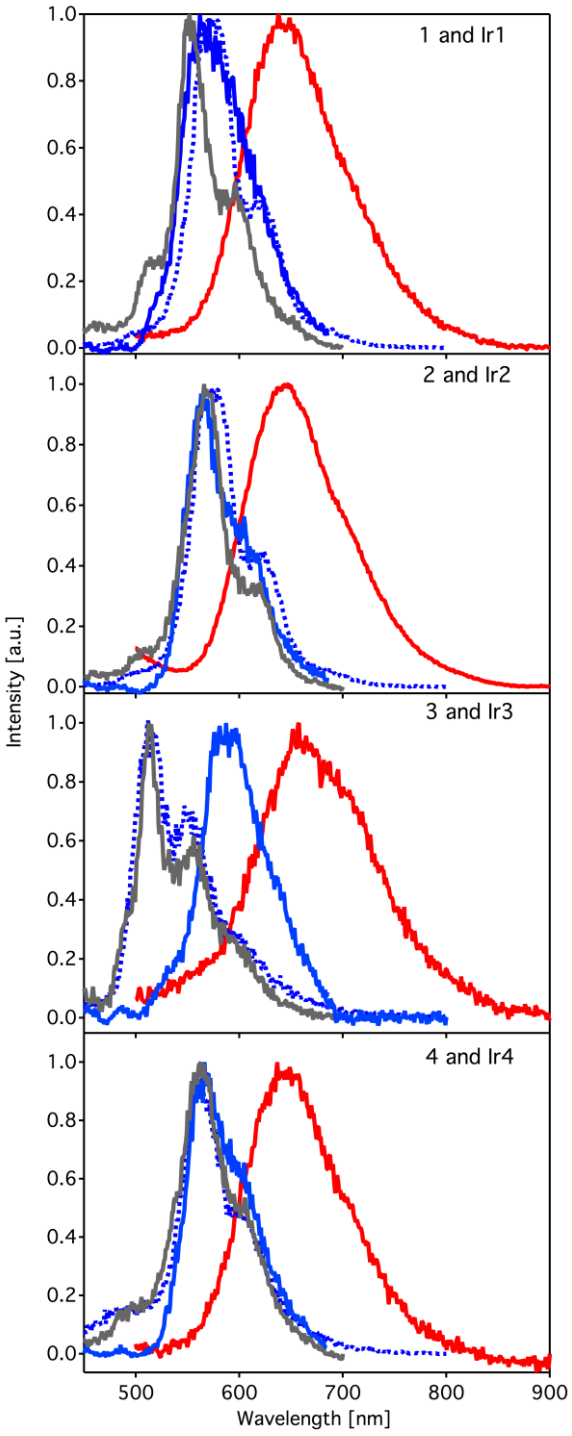


**Figure S1.** Normalized luminescence spectra at $\lambda_{exc}$ = 375 nm for ligands **1**–**4**, in dichlorometane at 300 K measured with a 50 µs delay (gray line), and complexes **Ir1**–**Ir4**, in dichloromethane at 300 K (red line), and in ethanol glass at 77 K measured with a 5 µs (solid blue line) and 50 µs (dotted blue line) delay.

**Table S1.** Selected bond distances (in Å) and bond angles (in deg.) calculated for **Ir1**-**Ir4** in the singlet ground state ($S_0$) and in the lowest-energy triplet state ($T_1$).

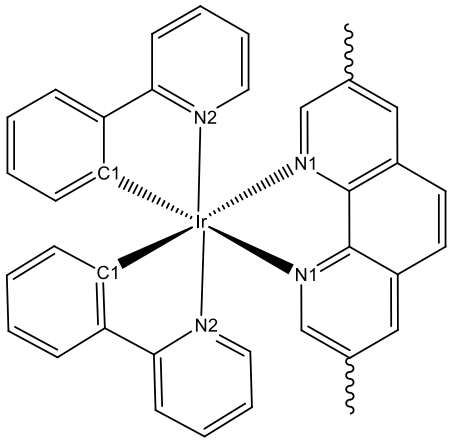


| | **Ir1** | | **Ir2** | | **Ir3** | | **Ir4** | |
|---|---|---|---|---|---|---|---|---|
| | $S_0$ | $T_1$ | $S_0$ | $T_1$ | $S_0$ | $T_1$ | $S_0$ | $T_1$ |
| Ir–$N_1$ | 2.227 | 2.222 | 2.227 | 2.223 | 2.224 | 2.224 | 2.227 | 2.224 |
| Ir–$N_2$ | 2.085 | 2.085 | 2.085 | 2.085 | 2.085 | 2.086 | 2.085 | 2.085 |
| Ir–$C_1$ | 2.023 | 1.994 | 2.023 | 1.994 | 2.023 | 1.993 | 2.023 | 1.994 |
| | | | | | | | | |
| $N_1$–Ir–$N_1$ | 75.5 | 75.5 | 75.5 | 75.5 | 75.5 | 75.4 | 75.5 | 75.5 |
| $C_1$–Ir–$N_2$ | 80.0 | 80.9 | 80.0 | 80.9 | 80.0 | 80.9 | 80.0 | 80.9 |

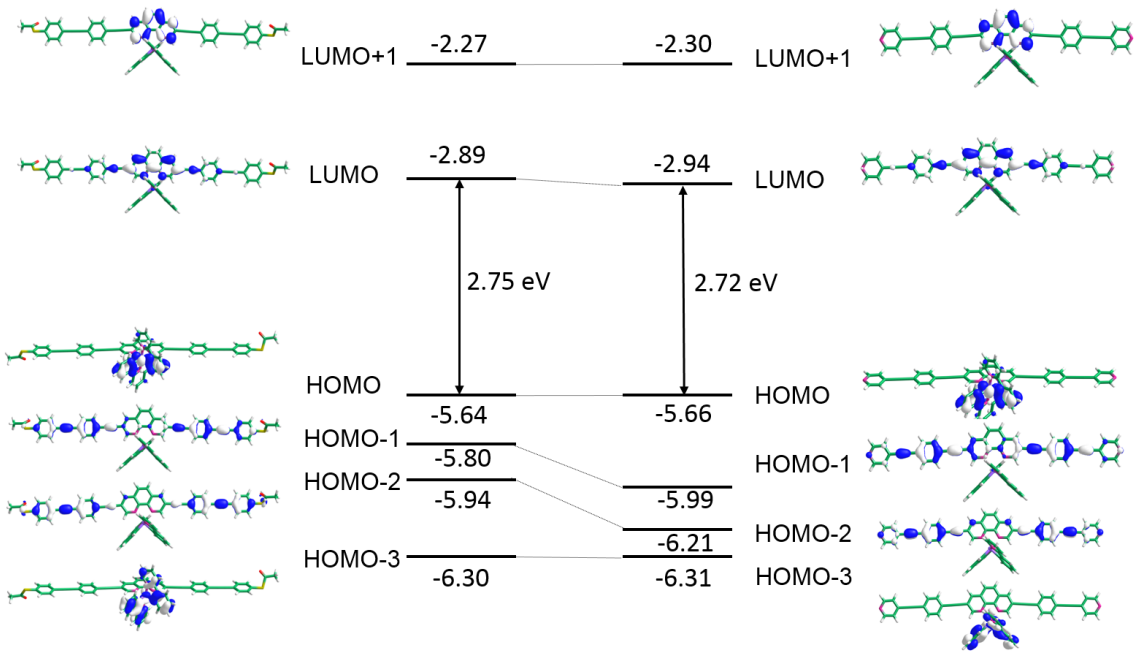


**Figure S2.** Schematic representation showing the electron-density contours (0.03 e bohr$^{-3}$) and the energy values (in [eV]) calculated for the highest occupied and lowest unoccupied molecular orbitals of **Ir2** and **Ir4**.

**RMN spectra:**

**1**

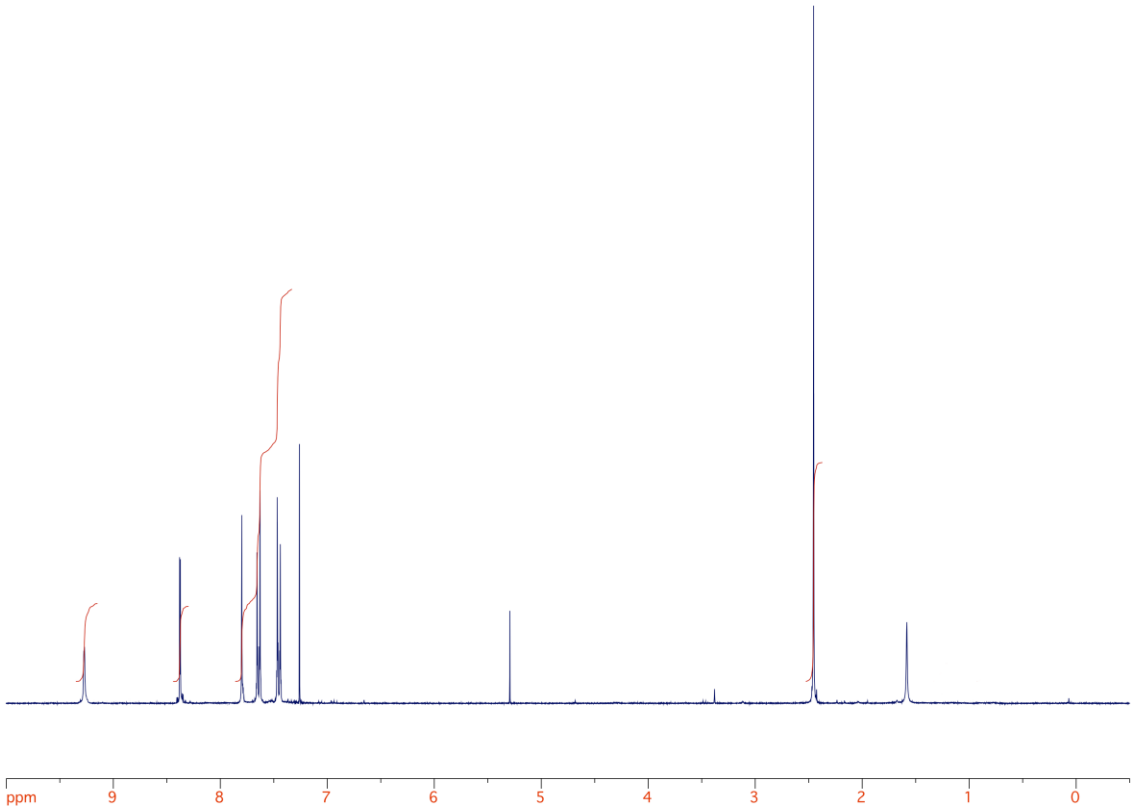


**2**

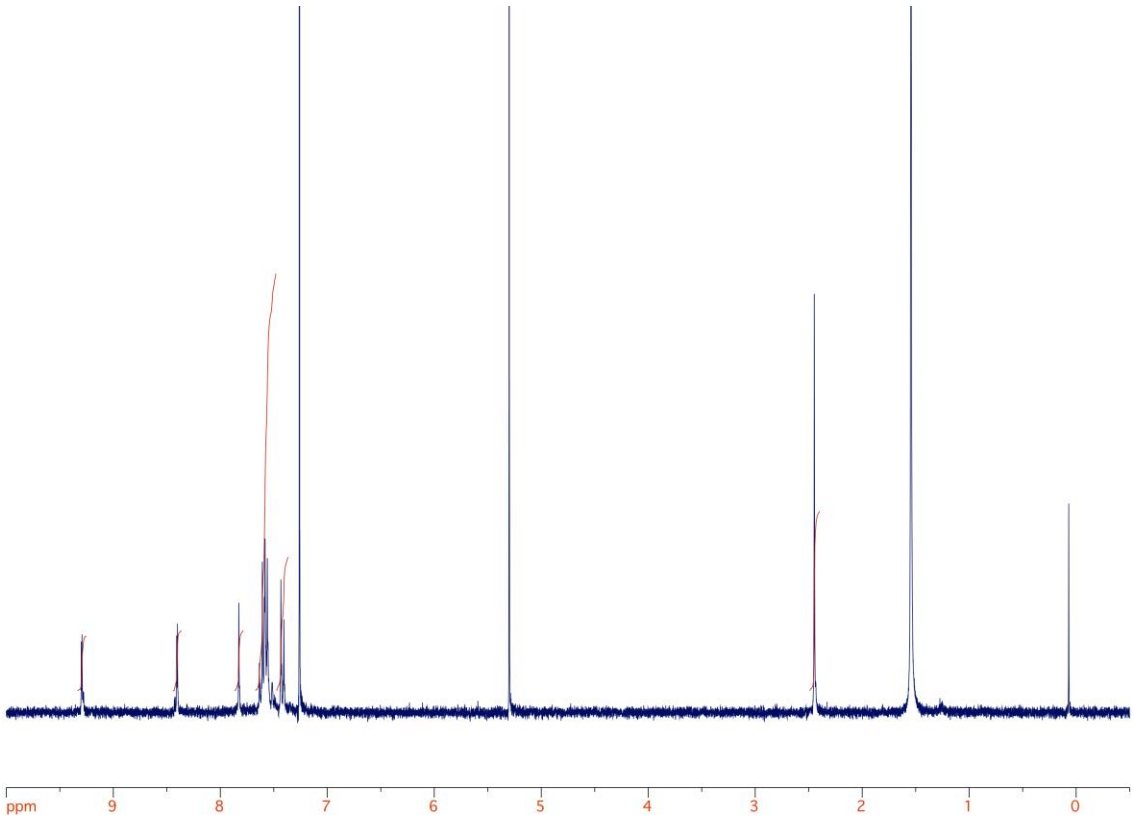

**3**

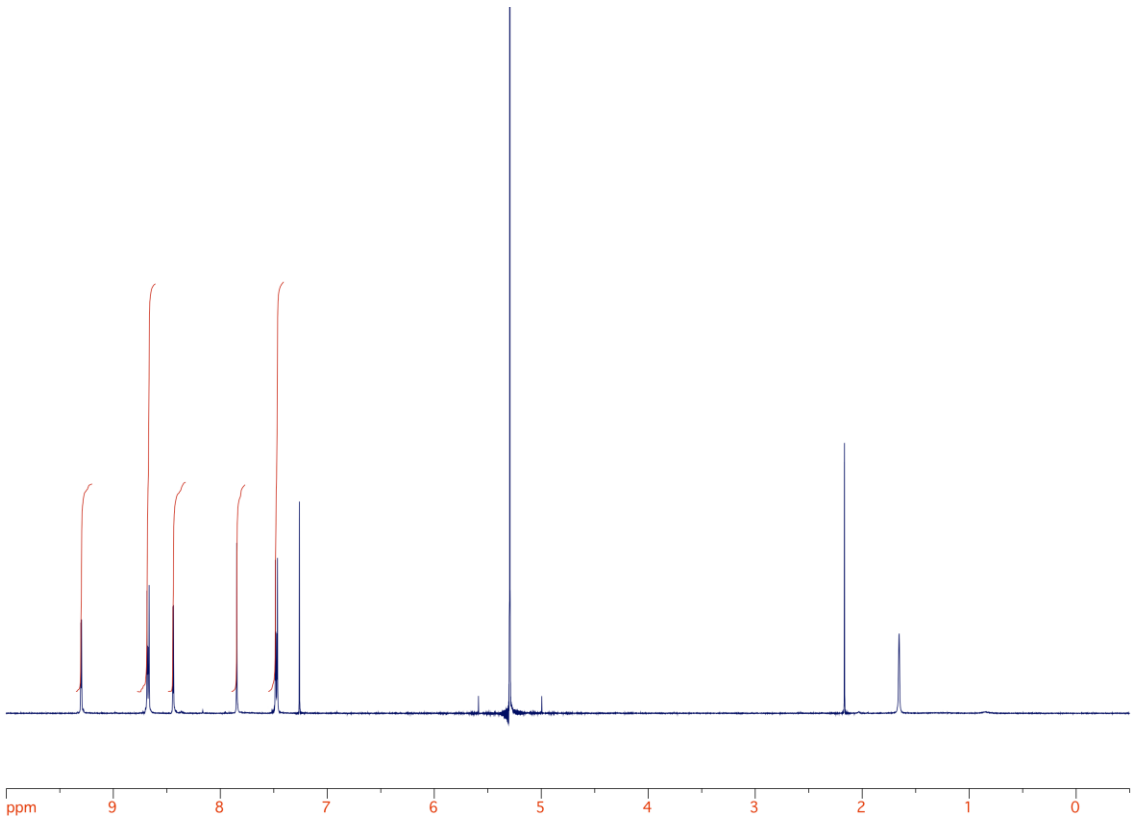


**4**

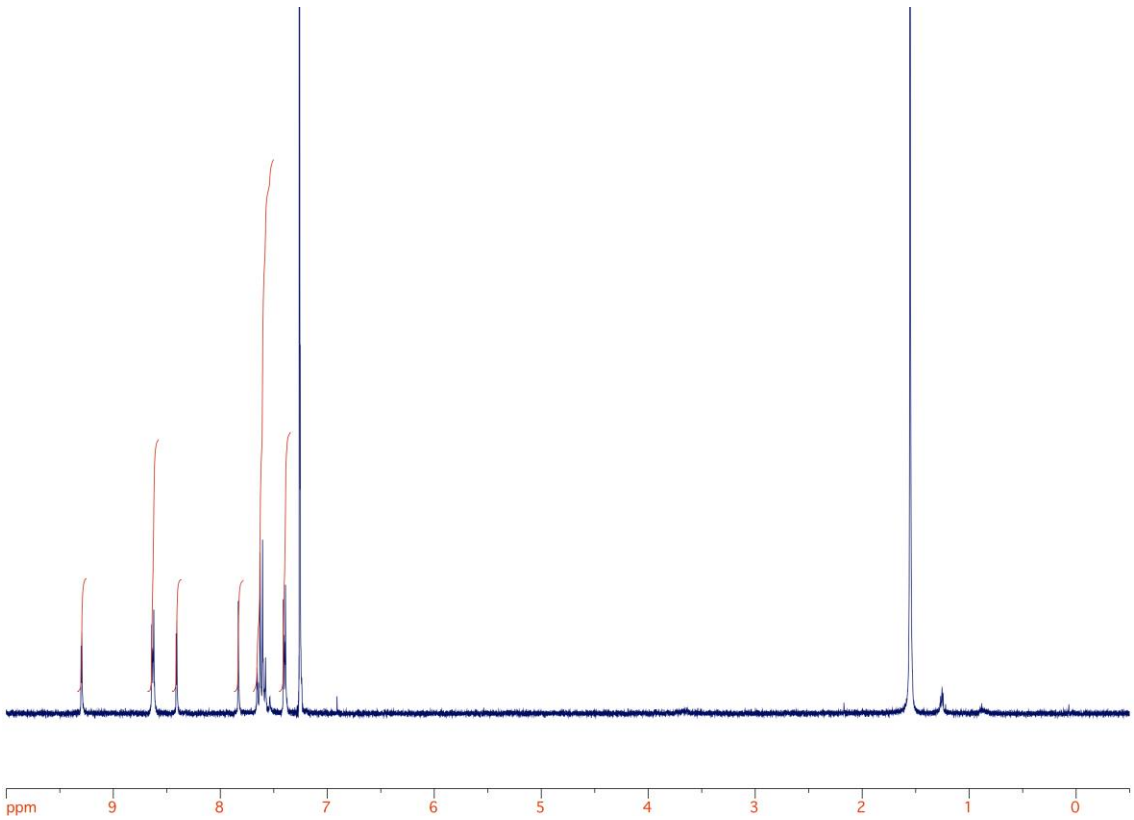

**Ir1**

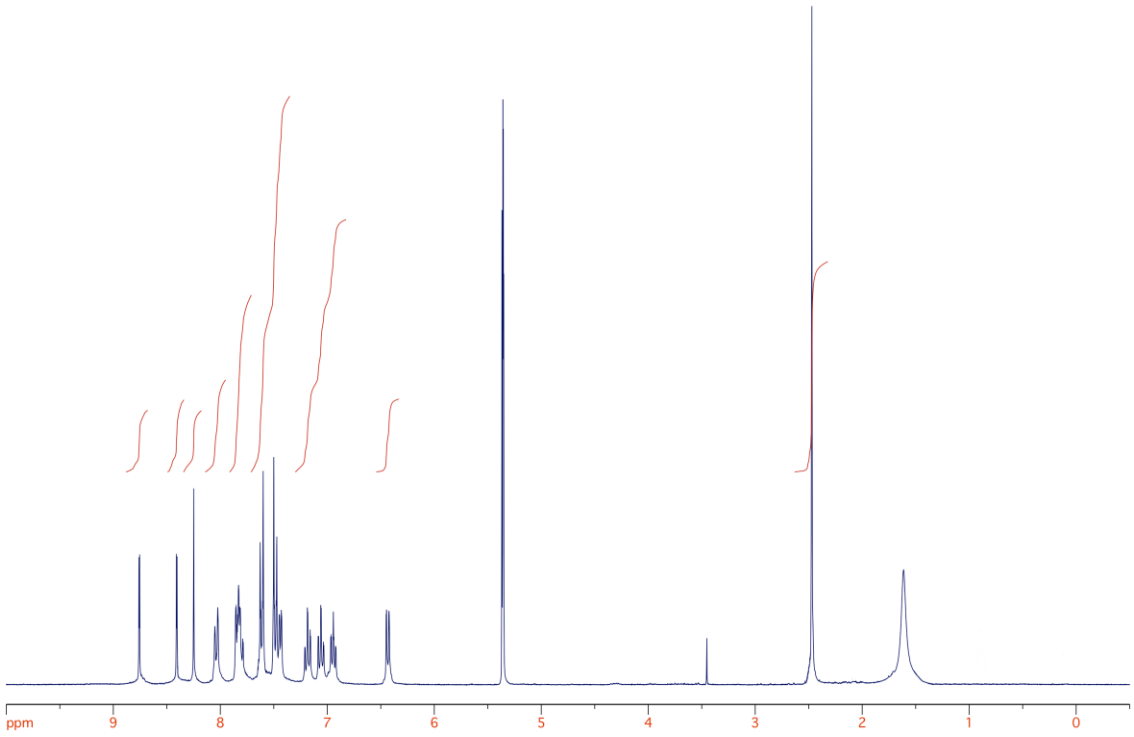


**Ir2**

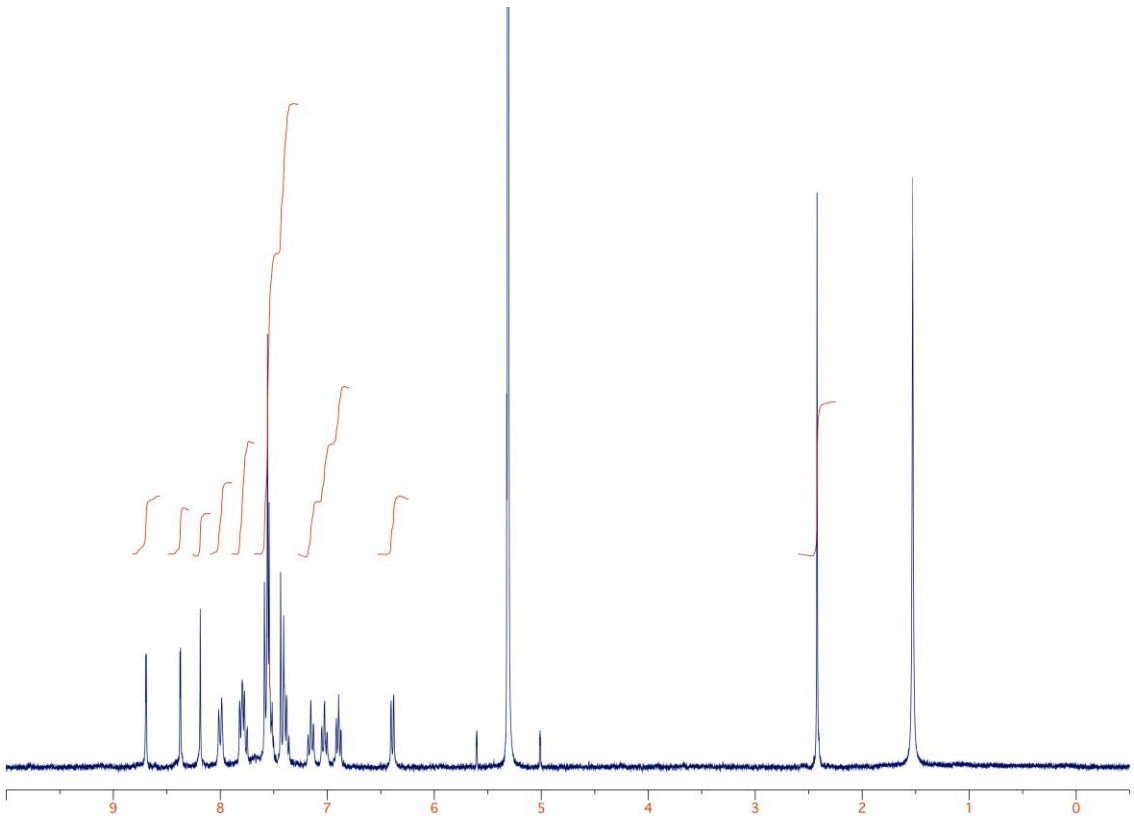

**Ir3**

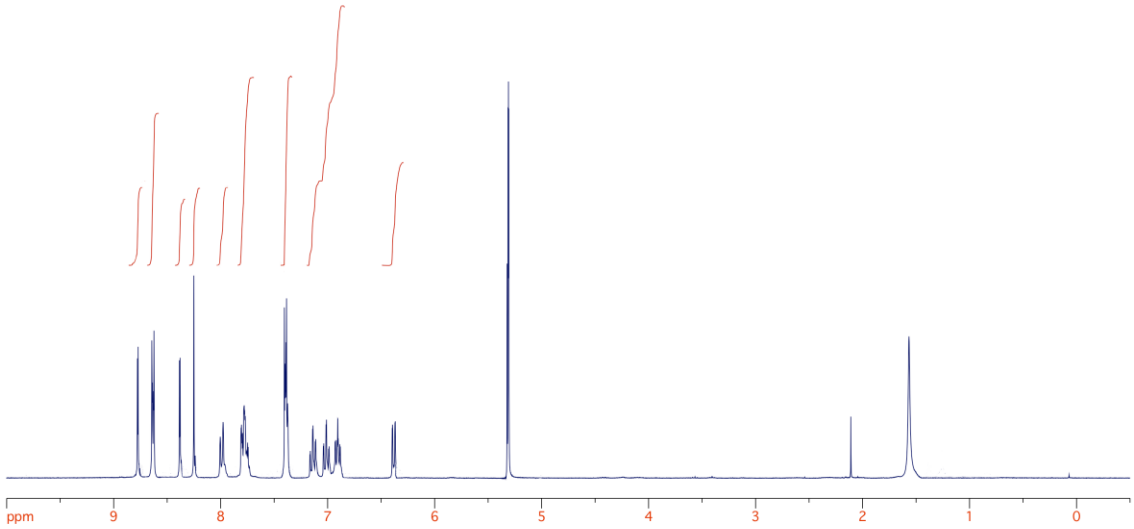


**Ir4**